

AFWL-TR-75-115

AFWL-TR-
75-115

2

FL

AD A031159



AN EXPERIMENTAL STUDY OF THE NONLINEAR PROPAGATION OF AN ELECTROMAGNETIC PULSE THROUGH THE IONOSPHERE

University of Arizona
Tucson, Arizona 85721

July 1976

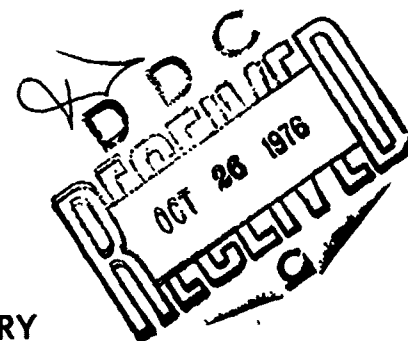
Final Report

Approved for public release; distribution unlimited

This project has been partially supported by the Defense Nuclear
Agency under DNA Subtask R99QAXEA091, Work Unit 42, Work Unit
Title: High Altitude Predictions.

Prepared for
Director
DEFENSE NUCLEAR AGENCY
Washington, DC 20305

AIR FORCE WEAPONS LABORATORY
Air Force Systems Command
Kirtland Air Force Base, NM 87117



6430

This final report was prepared by the University of Arizona, Tucson, Arizona, under Contract F29601-74-C-0110, Job Order WDNE0710 with the Air Force Weapons Laboratory, Kirtland Air Force Base, New Mexico. Captain William A. Seidler (ELP) was the Laboratory Project Officer-in-Charge.

When US Government drawings, specifications, or other data are used for any purpose other than a definitely related Government procurement operation, the Government thereby incurs no responsibility nor any obligation whatsoever, and the fact that the Government may have formulated, furnished, or in any way supplied the said drawings, specifications, or other data, is not to be regarded by implication or otherwise, as in any manner licensing the holder or any other person or corporation, or conveying any right or permission to manufacture, use, or sell any patented invention that may in any way be related thereto.

This report has been reviewed by the Information Office (OI) and is releasable to the National Technical Information Service (NTIS). At NTIS, it will be available to the general public, including foreign nations.

This technical report has been reviewed and is approved for publication.

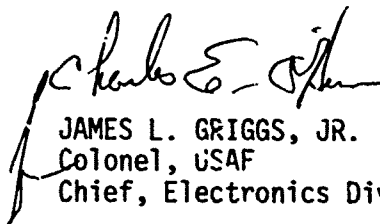


WILLIAM A. SEIDLER, II
Captain, USAF
Project Officer

FOR THE COMMANDER



LARRY W. WOOD
Lt Colonel, USAF
Chief, Phenomenology and Technical
Branch



JAMES L. GRIGGS, JR.
Colonel, USAF
Chief, Electronics Division

DO NOT RETURN THIS COPY. RETAIN OR DESTROY.



UNCLASSIFIED

SECURITY CLASSIFICATION OF THIS PAGE (When Data Entered)

REPORT DOCUMENTATION PAGE		READ INSTRUCTIONS BEFORE COMPLETING FORM	
1. REPORT NUMBER AFWL-TR-75-115	2. GOVT ACCESSION NO.	3. PERFORMING ORG. REPORT NUMBER	
4. TITLE (and Subtitle) AN EXPERIMENTAL STUDY OF THE NONLINEAR PROPAGATION OF AN ELECTROMAGNETIC PULSE THROUGH THE IONOSPHERE		5. TYPE OF REPORT & PERIOD COVERED FINAL REPORT JUN 74 - JAN 75	
7. AUTHOR(s)		8. CONTRACT OR GRANT NUMBER(s) F29601-74-C-0110 NEW	
9. PERFORMING ORGANIZATION NAME AND ADDRESS University of Arizona Tucson Arizona 85721		10. PROGRAM ELEMENT, PROJECT, TASK AREA & WORK UNIT NUMBERS 62707H WDNE0710, DC:XEC	
11. CONTROLLING OFFICE NAME AND ADDRESS Director Defense Nuclear Agency Washington, DC 20305		12. REPORT DATE Jul 1976	
14. MONITORING AGENCY NAME & ADDRESS (if different from Controlling Office) Air Force Weapons Laboratory Kirtland Air Force Base, NM 87117		13. NUMBER OF PAGES 72	
		15. SECURITY CLASS. (of this report) UNCLASSIFIED	
		15a. DECLASSIFICATION/DOWNGRADING SCHEDULE	
16. DISTRIBUTION STATEMENT (of this Report) Approved for public release; distribution unlimited. DNA-NWED-QAXE			
17. DISTRIBUTION STATEMENT (of the abstract entered in Block 20, if different from Report) A091			
18. SUPPLEMENTARY NOTES This project has been partially supported by the Defense Nuclear Agency under DNA Subtask R99QAXEA091, Work Unit 42, Work Unit Title: High Altitude Predictions.			
19. KEY WORDS (Continue on reverse side if necessary and identify by block number) Electromagnetic Pulse (EMP) High Altitude EMP EMP Prediction Techniques.			
20. ABSTRACT (Continue on reverse side if necessary and identify by block number) This report is concerned with the experimental investigation of EMP propagation through the D-region of the ionosphere. High and low amplitude EMP signals can propagate into space and pose a potential threat to satellites. The Air Force Weapons Laboratory (AFWL) has developed a theory which predicts that when an EMP propagates through the D-region of the ionosphere, that considerable energy can be absorbed from this pulse, thus reducing its potential threat. We have built a plasma machine in which pulse propagation in the ionosphere can be simulated.			

UNCLASSIFIED

SECURITY CLASSIFICATION OF THIS PAGE(When Data Entered)

ABSTRACT (Cont'd)

A TEM waveguide is immersed in a nitrogen plasma. We apply a pulse simulating an EMP to the input and observe the received signal at the output. A probe, which can measure the electron distribution function, allows us to monitor the electron temperature. Thus, energy absorbed from the pulse and electron temperature can be monitored. Other diagnostic systems allow many other quantities to be monitored.

ACCESSION FOR	
RTIS	White Section <input checked="" type="checkbox"/>
DDC	Blue Section <input type="checkbox"/>
UNCLASSIFIED	
JUSTIFICATION	
BY	
DISTRIBUTION/AVAILABILITY CODES	
Doc.	MAIL
A	

UNCLASSIFIED

SECURITY CLASSIFICATION OF THIS PAGE(When Data Entered)

SUMMARY

An experiment has been performed which demonstrated that electron temperatures and plasma effects similar to those predicted for electromagnetic pulses (EMP) propagating in the high altitude source region and D-region of the ionosphere can be maintained and observed in a laboratory experiment. Scaling laws have been developed which allow a long propagation path to be modeled by a one meter TEM waveguide emersed in a laboratory plasma. It has been demonstrated that nonlinear collision absorption processes and electron avalanche do occur as qualitatively predicted. The data collected in this experiment shows that absorption of energy from propagating signals can occur and frequencies appreciably above the plasma frequency.

PREFACE

The theoretical work underlying the experimental effort described in this report has been developed by Capt. William A. Seider at the Air Force Weapons Laboratory, Kirtland AFB, New Mexico. The plasma machine and the experimental program herein described has proceeded under the direction of Dr. Robert N. Carlile, Professor of Electrical Engineering, Department of Electrical Engineering, University of Arizona, Tucson, Arizona. Three graduate students have been involved with the development of this equipment: Robert A. Piejak, PhD candidate; Gary L. Jackson, PhD candidate, and Gary L. Hagedon, MS candidate.

TABLE OF CONTENTS

	<u>Page</u>
I INTRODUCTION	1
II THEORY OF ELECTRON HEATING OF THE D-REGION BY AN EMP	2
III GENERAL DESCRIPTION OF EXPERIMENT	6
IV GENERAL DESCRIPTION OF SYSTEMS COMPONENTS	15
V DESCRIPTION OF THE EQUIPMENT THAT HAS BEEN BUILT UNDER AIR FORCE CONTRACT	20
VI PRELIMINARY RESULTS	28
VII RECOMMENDATIONS FOR FUTURE WORK	32
REFERENCES	35

I. Introduction

High and low amplitude electromagnetic pulse (EMP) signals can propagate into space and pose a potential threat to satellites. At the Air Force Weapons Laboratory, (AFWL), a theory has been developed which predicts that a large amplitude EMP signal propagating through the D-region of the ionosphere will cause rapid heating of the electron in this region, resulting in conditions being such that considerable energy is absorbed from the pulse. This absorption would thus reduce the potential threat of the EMP to satellites.

In June, 1974, the Air Force contracted with The University of Arizona to build an experimental machine that would allow the AFWL theory to be tested experimentally. During the 6-month technical phase of the contract, the emphasis has been, of necessity, on the construction of the machine. On January 15, 1975, when this phase ended, the machine had been constructed, and some preliminary data had been obtained from it. This report describes the machine in detail and presents these preliminary data.

In Section II of this report, a summary of the theory developed at AFWL is presented. In Section III, a general description of the experimental procedure that will lead to a testing of the theory is given, including a discussion of scaling between the ionospheric plasma and the laboratory plasma. In Section IV the features of the machine are discussed in somewhat general terms. In Section V, the details of the construction

of the machine are presented, and in Section VI, there is given the preliminary experimental results as of January 15, 1975. Finally, Section VII gives some recommendations for future work.

II. Theory of Electron Heating of the D-Region by an EMP

A theory developed at the Air Force Weapons Laboratory predicts electron heating of the D-region by an EMP. A summary of that theory is presented here^[1]. Note that all figures in this Section are from Reference 1.

To summarize the theory in words, consider a large amplitude fast risetime EMP, incident upon the lower edge of the D-region (low altitude edge). As the pulse starts to propagate through the D-region, it sets up a conduction current density \bar{J} . The current density \bar{J} results in joule heating of the electrons at a rate of $\bar{J} \cdot \bar{E}$ joules per second per m^3 . This energy, absorbed by the electrons from the EMP, is ultimately transferred to the neutrals.

Joule heating of the electrons roughly increases with altitude in the D-region, so that the energy in the pulse declines at first slowly, and then rapidly as altitude increases. The rate at which energy is transferred to neutrals versus the rate at which it is absorbed from the pulse is such that the electron temperature reaches a peak around 85 km which may be of the order of several hundred electron volts if the pulse amplitude is high enough. These high electron energies cause electron avalanching to occur so that the electron number density will increase. The avalanche-produced electrons will contribute to \bar{J} . Nearly total absorption of the pulse can occur by the time the pulse emerges from the high altitude side of the D-region.

The starting point for the theory is the first three moments of the Boltzmann equation and Maxwell's equations:

$$\frac{\partial n_e}{\partial t_s} = \rho v_i (T_e) n_e \quad (\text{First Moment}) \quad (1)$$

$$\frac{\partial \bar{v}}{\partial t_s} = -\frac{e}{m} (\bar{E} + \bar{v} \cdot \bar{B}) - \rho v_m (T_e) \bar{v} - \rho v_i (T_e) \bar{v} \quad (\text{Second Moment}) \quad (2)$$

$$\frac{\partial T_e}{\partial t_s} = -\frac{2}{3} \bar{v} \cdot \bar{E} - \rho v_w (T_e) (T_e - T_{eo}) - \rho v_i (T_e) T_e \quad (\text{Third Moment}) \quad (3)$$

Maxwell's equations:

$$\epsilon_0 \frac{\partial E_r}{\partial t_s} = J_r \quad (4)$$

$$\frac{\partial (E_\theta r)}{\partial r} = \frac{\mu_0 c r}{2} J_\theta \quad (5)$$

$$\frac{\partial (E_\phi r)}{\partial r} = \frac{\mu_0 c r}{2} J_\phi \quad (6)$$

$$\frac{\partial (B_\theta r)}{\partial r} = -\frac{1}{2} \mu_0 r J_\phi \quad (7)$$

$$\frac{\partial (B_\phi r)}{\partial r} = \frac{1}{2} \mu_0 r J_\theta \quad (8)$$

The system is shown in Fig. 1. In Equations (1) through (8), n_e is the number density, \bar{v} is the average velocity, \bar{E} is the amplitude of the EMP.

$\bar{J} = -n_e e \bar{v}$ is the current density, T_e is the electron energy expressed in

electron volts, and \bar{B} is the magnetic field. These quantities are all functions of the retarded time t_s only. \bar{B} can contain a DC part due to the earth's magnetic field. All quantities except T_e are expressed in terms of their usual MKS units. When v_i , v_m , and v_w are multiplied by c , the number density of neutrals, the results are collision frequencies. These are associated with collision cross sections for electron generation through avalanching, momentum transfer, and energy transfer to neutrals, respectively. They are functions of the electron temperature. T_{eo} is the ambient electron temperature. Other constants should be self-evident.

The transformation to retarded time is made,

$$t_s = t - r/c \quad (9)$$

where t is clock time and c is the velocity of light^[2]. According to this transformation, $\partial/\partial t$ is replaced by

$$\partial/\partial t_s \quad (10)$$

and ∇ is replaced by

$$\nabla - \hat{r}(1/c) \partial/\partial t_s \quad (11)$$

where r points from the source point to (r, θ, ϕ) . [See Fig. 1.]

After this transformation has been made, it is possible to show that variation of the dynamical variables with r is much slower than variation with ct_s . We can then neglect spatial derivatives compared to derivatives with respect to t_s . Equations (1) through (8) have been transformed according to the procedure described above.

The D-region is subdivided into incremental lengths along the r axis in Fig. 1 of 10 km each, corresponding to an incremental altitude

change of about 1 km. An ambient number density n_{eo} and temperature T_{eo} is assigned to each increment. An electric field (Fig. 2) is applied to the input to the first increment, which occurs at 52 km. Four different cases have been considered at AFWL, indicated by the four pulses labeled A, B, C, and D in Fig. 2.

A computer iterative technique was used to determine the response of the plasma to the pulse, and effect of the plasma to the pulse. Consider an increment whose input is at r_n and output is at r_{n+1} . Call this the n^{th} increment. By keeping the electric field at the input to the previous six increments, a Taylor series could be constructed to determine the electric field at r_{n+1} . This electric field is then used in the plasma Equations (1) through (3) as a source to find \bar{v} , T_e and n_e as a function of t_s . The boundary conditions on these equations are:

$$\begin{aligned} \text{At } t_s &= 0, \\ \bar{v} &= 0, \\ T_e &= T_{eo}, \\ n_e &= n_{eo}. \end{aligned}$$

From this, \bar{J} is computed, and using (4) through (6), a correction to \bar{E} at r_{n+1} is found. This process is repeated using the corrected \bar{E} such that a further correction in \bar{E} is calculated. This procedure repeats until \bar{E} at r_{n+1} stabilizes.

The results of this procedure applied to nitrogen ionosphere can be summarized as follows. The percent of total energy stored in the pulse as a function of altitude is shown in Fig. 3. Most of it remains in the pulse until about 80 km, and thereafter, it is rapidly absorbed by the

electrons. The high amplitude pulses (A, B, and C) retain their energy longer on a percentage basis than the low amplitude pulse D.

In the wake of the pulse, the energy density in the D-region (located both in neutrals and electrons) calculated at AFWL is shown in Fig. 4. It generally increases with altitude. This energy is divided between the electrons and neutrals. The rate at which energy is flowing into the neutrals is shown in Fig. 5.

Energy flows to the electrons from the pulse at a greater rate than it is absorbed from the electrons by the neutrals. This causes the electrons to increase in temperature. The peak temperature achieved by the electrons is shown in Fig. 6. It is seen that for the high amplitude pulse, an electron temperature of nearly 100 ev is achieved.

III. General Description of Experiment

The D-region of the ionosphere is characterized by low electron densities (100 electrons per cm^3 for a sunspot minimum, night time ionosphere). For a collisionless plasma, frequencies below 9×10^4 MHz would be reflected. As we have seen in the preceding section, the theory developed at AFWL has indicated that in the D-region, a nonlinear absorption can occur which affects frequencies considerably higher.

We have conceived of an experiment which allows pulse propagation in the ionosphere to be simulated, and which will permit theoretical predictions of Section II to be tested. In brief, a TEM waveguide is immersed in a nitrogen plasma. We apply a pulse simulating an EMP at the input and observe the received signal at the output. We measure the real time variation of the input and output pulses with a sampling scope.

The TEM waveguide, which is about 1 meter long, simulates an incremental distance in the D-region of the order of 1 kilometer. This would correspond to one iteration interval of the AFWL theory.

We can measure, by means of an electrostatic analyzer probe, the electron distribution function. This allows us to measure the maximum energy of electrons, which the theory predicts can exceed 100 ev. In addition, in principle, we should be able to obtain from the distribution function, the final values of the electron density and drift velocity after electron heating by the EMP.

Ambient values (pre-pulse) of electron density and electron temperature are measured by standard electromagnetic cavity perturbation and Langmuir probe techniques.

We need to discuss the correspondence between the behavior of the pulse propagating in our laboratory plasma and that of a pulse propagating in the ionosphere. We make a correspondence between our 1 meter length plasma filled waveguide and an incremental distance in the ionosphere discussed in Section II. The laboratory plasma is uniform and we assume that the ionospheric plasma over the distance increment is also uniform.

We now discuss the determining Equations (1) through (8) without reference to a particular system. It is assumed that these equations are valid for either system.

The uniform plasma is characterized by an ambient number density n_{eo} and electron temperature T_{eo} electron volts. From these, we may construct the following constants:

- (1) The ambient thermal velocity:

$$v_t \equiv [e T_{eo} / m]^{1/2} \quad (12a)$$

(2) The ambient plasma frequency:

$$\omega_p = [n_{eo} e^2 / m \epsilon_o]^{1/2} \quad (12b)$$

(3) The electron cyclotron frequency

$$\omega_c = e B_o / m \quad (12c)$$

derived from the DC magnetic field:

$$\vec{B} = \hat{u} B_o \quad (12d)$$

(4) The debye length:

$$\lambda_D = V_t / \omega_p \quad (12e)$$

(5) The ambient electron momentum collisions frequency:

$$\nu = \rho \nu_m (T_{eo}) \quad (12f)$$

We may now define two normalized independent variables

$$\tau = \omega_p t_s \quad (13a)$$

and

$$R = r / \lambda_D \quad (13b)$$

and five normalized dependent variables:

$$N \equiv n_e / n_{eo} \quad (14)$$

$$T \equiv T_e / T_{eo} \quad (15)$$

$$\bar{V} \equiv \bar{v} / V_t \quad (16)$$

$$\bar{E} = \frac{(e/m)\bar{E}}{\omega_p V_t} \quad (17)$$

$$\bar{B} = \frac{(e/m)\bar{B}}{\omega_p} \quad (18)$$

which are functions of τ . We also define the auxiliary function

$$F_i(T_{eo}, T) = v_i(T_e)/v_m(T_{eo})$$

$$F_m(T_{eo}, T) = v_m(T_e)/v_m(T_{eo})$$

and

$$F_w(T_{eo}, T) = v_w(T_e)/v_m(T_{eo})$$

The set of Equations (1) through (8) may now be put into normalized form by multiplying each equation by the following factor:

$$(1) \text{ by } (n_{eo} \omega_p)^{-1}$$

$$(2) \text{ by } (V_t \omega_p)^{-1}$$

$$(3) \text{ by } (T_{eo} \omega_p)^{-1}$$

$$(4) \text{ by } (e/m)/V_t \omega_p^2$$

$$(5) \text{ and } (6) \text{ by } (e/m)\lambda_D/V_t \omega_p$$

$$(7) \text{ and } (8) \text{ by } (e/m)\lambda_D/\omega_p$$

The results are:

(Plasma Equations)

$$\frac{dN}{d\tau} = \frac{v}{\omega_p} F_i N \quad (19)$$

$$\frac{dV}{d\tau} = -\bar{E} - \bar{V} \cdot \bar{B} - \frac{\omega_c}{\omega_p} \bar{V} \cdot \hat{u} - \frac{v}{\omega_p} \bar{V} [F_m + F_i] \quad (20)$$

$$\frac{dT}{d\tau} = -\frac{2}{3} \bar{V} \cdot \bar{E} - \frac{v}{\omega_p} F_w (T - 1) - \frac{v}{\omega_p} F_i T \quad (21)$$

(Maxwell's Equations)

$$\frac{\partial E_r}{\partial \tau} = -N V_r \quad (22)$$

$$\frac{1}{R} \frac{d}{dR} (R E_\theta) = -\frac{1}{2} \frac{V_t}{c} N V_\theta \quad (23)$$

$$\frac{1}{R} \frac{d}{dR} (R E_\phi) = -\frac{1}{2} \frac{V_t}{c} N V_\phi \quad (24)$$

$$\frac{1}{R} \frac{d}{dR} (R B_\theta) = \frac{1}{2} \frac{V_t^2}{c^2} N V_\phi \quad (25)$$

$$\frac{1}{R} \frac{d}{dR} (R B_\phi) = -\frac{1}{2} \frac{V_t^2}{c^2} N V_\theta \quad (26)$$

The electric field at the input to the ionospheric increment or to the waveguide has an amplitude E_0 and a rise time t_r and fall time t_f . Suppose that we require that for both systems, the following system parameters all be the same:

$$\frac{e}{m} E_0 / \omega_p V_t, \omega_p t_r, \omega_p t_f, \frac{v}{\omega_p}, \frac{\omega_c}{\omega_p}, \frac{V_t}{c}, F_m, F_v, \text{ and } F_i \quad (27)$$

Then the normalized equations will look the same for either system, and their solution will be identical of either system. To restate: if the system parameters listed in (27) can be made the same for both systems, then the two systems will behave in exactly the same way. The normalized independent variables versus the independent variables τ and R will be the same, and if this set of normalized independent variables can be found, say, in the laboratory system, the unnormalized variables in the ionosphere can be found from (14) through (18).

This result is much more general than indicated here. The previous discussion has made use exclusively of the retarded time and not the usual clock time. However, we have shown elsewhere that if one starts with the Boltzmann equation and Maxwell's equation not transformed by retarded time, but using usual clock time, the conclusions are the same; i.e., if the quantities in (27) are the same for both systems, normalized dependent variables will behave in the same way in both systems versus the independent variables τ and $R \equiv \tau/\lambda_D$. All nonlinear effects are encompassed, as well as such phenomena as Landau damping.

We consider next the practicality of making the nine quantities and functions in (27) the same in the laboratory and ionospheric systems. Consider the first five, all containing ω_p , which tends to be low in the ionosphere (90 KHz), but which can conveniently be at least 9 MHz in the laboratory. If S is a scale factor, i.e., the ratio of ω_p in the laboratory to that in the ionosphere, then in the laboratory, time t_s is scaled down by S including t_r and t_f while E_0 is scaled up.

Specifically, if E_o , t_r , t_f , v , and ω_c are the ionospheric values, the correct values for the laboratory are SF_o , t_r/S , t_f/S , Sv , and $S\omega_c$. In the laboratory, E_o , t_r , and t_f can be varied by design of the pulse generator as described in Section V, while v and ω_c can be varied by means of the pressure and confining magnetic field. Since these quantities can be changed over wide limits, the appropriate scaled values can be usually achieved.

It is the remaining four quantities which are difficult to scale. V_t , F_i , F_m , and F_w depend on T_{eo} . Thus, T_{eo} must be the same in both systems. In our steady state plasma, T_{eo} is about 1 ev and cannot be easily controlled, while in the D-region, it is about .01 ev. Thus, V_t/c will be about a factor of 30 larger in the laboratory, and the functions F_m , F_w , and F_i will be somewhat different functions of T in the ionosphere than in the laboratory, particularly F_i . Thus, exact correspondence of the quantities in (27) is not possible in the ionosphere and laboratory.

However, the purpose of this work is to test the validity of the theory in Section II. To this end, the information about scaling above can be put to the following use:

A computer run should be made with T_{eo} set equal to 1 ev for one distance increment and ω_p , E_o , t_r , t_f , v , and ω_c chosen such that a) the scaled values are attainable in our laboratory machine, b) the theoretically predicted results show electron temperature approaching 100 ev. The results from this run can now easily be scaled to predict our experimental results for a range of ω_p in our laboratory plasma.

In the machine which we have built, the plasma is confined by a magnetic field as described in Section IV. However, according to the Statement of Work for this contract, the theory to be tested initially

assumes zero magnetic field. The reader is referred to Item 6.1 and Equations (1) through (4) in Item 3.2 of the Statement of Work. This presents no problem at medium to high altitudes in the D-region since we can make ω_p large enough and ω_c small enough that the ratio ω_c/ω_p is less than 0.1. Over the length of the TEM waveguide, such a low magnetic field will have negligible effect.

At lower altitudes, we could use a discharge plasma system which has not been built as of January 15, 1975 (but which could be added at small expense, about \$500). In this case, the plasma is confined by a glass pipe, and no magnetic field is required. This will be a truly zero magnetic field plasma.

However, it is quite easy to take into account the earth's magnetic field. AFWL has completed a theory which includes this magnetic field^[1]. We must require that the direction of the magnetic field should be parallel to the direction of propagation. We can do this by using the electron beam-generated plasma system and letting the magnetic field which confines the plasma have an appropriate value. To use the existing flat plate TEM waveguide, the magnetic field must be such that the electric field does not demonstrate Faraday rotation significantly over the length of the waveguide. The theoretical data presently available from AFWL show that for typical magnetic fields found in the D-region this will not happen.

For a strictly zero DC magnetic field, and perfectly conducting planes, the fields of the pulse in the waveguide are exactly TEM fields with identical electric and magnetic field configurations and dispersion curve to that which would be found in an infinite cross-section of ionospheric plasma^[3]. We do not use perfectly conducting planes, but rather planes consisting of stainless steel wire mesh. We assume that the fineness

of the mesh (compared to the shortest wavelength component of the pulse) and its slightly lossy character do not significantly alter the fields or dispersion curve.

The presence of a DC magnetic field will cause the fields to rotate (Faraday rotation). For the choice of parameters to be used in these experiments which are to simulate the ionosphere, Faraday rotation is evidently very slight, as has been demonstrated by the AFWL theory, e.g., if at the input to a distance increment, the electric field is entirely in the y direction (defined as normal to the waveguide planes), at the output, only a very small x and z (the axial direction) component has been generated. In our experimental system, these components cannot be measured. However, any changes in the y component we should be able to accurately measure.

The TEM waveguide plates are sufficiently separated so that avalanching may occur.

A Fourier analysis in time and space of the real time electric field would reveal that this electric field consists of short and long wavelength components. The long wavelength components are electromagnetic in character, and will propagate in the axial direction. The electric field will be directed, in the absence of a magnetic field, in the same direction as the electric field input pulse, namely, normal to the waveguide plates. Thus, the plates do not influence the propagation of these components.

It is possible that there will be short wavelength components, not predicted by the AFWL theory, which only exist in the nonlinear regime. These are electrostatic in character (e.g., Bernstein modes)^[4-8]. The

wavelength of these components is typically much shorter than the separation of the plates, so that again, the plates do not particularly influence these waves. For example, for Bernstein modes, collisional damping requires that λ , the wavelength for a Bernstein mode, satisfy

$$\lambda < \frac{2V_t}{f_c}$$

where V_t is defined by (12a) and f_c is $\omega_c/2\pi$ and ω_c , the cyclotron frequency is given by (12c). For our system, V_t is approximately 5×10^7 cm/sec and for the scaling that we have anticipated ($S = 310$), f_c is 300 MHz if we take into account the earth's magnetic field. This leads to

$$\lambda < .333 \text{ cm}$$

It is these short wavelength waves which are the result of plasma turbulence. Thus, the plates do not change the quantitative correspondence between the laboratory model and the ionosphere.

IV. General Description of System Components

The details of the system we have built will be described in the next section. Here we give a general overview of this system.

The system should contain two types of plasmas. The one which has been constructed at the present time we shall refer to as an electron beam-produced plasma system, while the other we shall call a discharge plasma system. These plasmas will be discussed below, as well as the TEM waveguide, the pulse generator, and the diagnostic systems.

A. Electron Beam-Produced Plasma

This plasma has been described in the literature^[9,10], and has been recently constructed at two major laboratories^[11, 12]. In Fig. 7

there is shown a grid-cathode arrangement followed by a long drift space at the end of which is a collector. The grid, which is close to the cathode, accelerates primary electrons emitted by the cathode. These pass through the grid with energies of typically 50 ev.

Now the entire volume of the system contains a gas of nitrogen at a low pressure. Further, an external solenoid produces an axial magnetic field. The primary electrons passing through the grid-cathode space are constrained to drift along a magnetic field line. In the drift space, they ionize gas atoms, producing secondary electrons with relatively low energies, typically 1 ev. A secondary electron and the positive ion produced when the secondary electron is removed from a neutral atom, also move along magnetic field lines. Typically, a primary 50 ev electron will produce several secondaries. The secondaries have approximately a Maxwellian velocity distribution. We have observed that if the collector is at grid potential, the primary electrons make one pass through the system and then are collected by the collector; if the collector is negative with respect to the grid, the primary electrons will make several passes.

Because the electrons are constrained to follow magnetic field lines, the plasma cross-section will be an image of the emitting surface of the cathode. Our system contains a 3-inch diameter dispenser-type cathode which gives a plasma cross-section whose electron density has cylindrical symmetry. The plasma has been observed to nicely fill the space between the TEM waveguide plates.

We shall now discuss the parameters attainable in this system. A series of external solenoids produce a magnetic field coaxial with the axis of the plasma. The magnetic field has a maximum steady-state value of 300

gauss. Within the plasma, the magnetic field is constant in time to $\pm 0.1\%$. The minimum magnetic field that can be attained while still confining the plasma is about 15 gauss. Thus, for a field variation of 15 to 300 gauss, the variation of the electron cyclotron frequency $\omega_c/2\pi$ is 40 MHz to 2.800 GHz.

The electron and ion number density depends on the gas pressure and on the grid-cathode current. The maximum number density is $10^{11}/\text{cm}^3$ and the minimum is determined by diffusion properties of the electrons, and is estimated to be about $10^6/\text{cm}^3$. This gives a range for the electron plasma frequency $\omega_p/2\pi$ of 8.98 GHz down to about 9 MHz.

The electron momentum transfer collision frequency ν depends on the kind of gas, electron temperature, and gas pressure. Nitrogen can be used without damaging the cathode. We can generally operate at pressures in the range 0.1 micron to 20 microns. For He, this corresponds to a collision frequency of ν of 10 MHz to 100 KHz, and undoubtedly higher collision frequencies than 10 MHz would be possible. For N_2 , it is roughly the same providing that the electron temperature T_{eo} is not a critical value of 2.2 ev. Then the collision frequency would be about a factor of five higher than those stated above. The electron temperature T_{eo} will be about 1 ev, and is not under our control.

B. Discharge Plasma

This plasma is produced in a large pyrex tube, which is rectangular in cross section where the TEM waveguide is located and which tapers to a round cross section beyond this region.

The tube is open at both ends. A cathode (1 inch in diameter, which we have on hand) protrudes into the round end. At the rectangular end

is a collector. By grounding the collector and making the cathode at a negative potential, it is well known that an arc discharge can be established which is contained by the glass tube. We have already mocked up this system using a round cross section tube with nitrogen gas and found that an arc discharge can easily be obtained.

The TEM waveguide plates set on the flat surfaces of the rectangular portions of the pyrex tube. They are external to the discharge. The details of construction may be seen in Section V.

The parameters obtainable in this type of plasma correspond to higher pressures, of the order of 10 microns or higher and number densities in the range 10^6 to 10^{10} . The electron temperature is about the same as in the electron beam-produced plasma, i.e., about 1 ev.

C. Pulse Generator

The pulse generator consists of a mercury reed switch in series with a DC power supply of voltage at the desired amplitude of the EMP and a coax line connected to the TEM waveguide input. It is opened by a magnetic field coil. The details are given in Section V. We have built a device which has a rise time of 100 picoseconds and a fall time which we can vary by the size of a metal slug in the system. Currently, the fall time is about 3 nanoseconds, but this can be altered. The largest amplitude we have introduced into the plasma loaded waveguide to date is 2000 volts. We have the capability of increasing this to nearly 10,000 volts. We do not know yet if arcing will occur at these high voltages.

D. TEM Waveguide

This waveguide consists of two parallel plates. Each is 7 centimeters wide, and they are separated by 3 centimeters wide such that the characteristic impedance in free space is 109 ohms. In the electron

beam-produced plasma, the plates are 1/4 inch mesh stainless steel screen while in the discharge plasma they are strips of 0.050 inch thick stainless sheet which will be screwed to the top and bottom of the pyrex glass discharge tube.

For either type of plasma, conical tapers provide a broad-band transition to a twin-lead transmission line which passes through the vacuum wall. The characteristic impedance of 109 ohms is maintained through the vacuum wall at both the input and output.

Outside the vacuum, broad-band tapers provide a transition from the 109 ohm twin-lead line to a 50 ohm coaxial cable. This cable attaches to the pulse generator at the input and, through a suitable termination, to the sampling scope at the output.

E. Electrostatic Analyzer Probe

In the presence of an EMP, the electrons will be heated such that their average energy far exceeds 1 ev. We are expecting peaks of average energy exceeding 100 ev. Furthermore, this type of heating may last only a short time; after the electrons are heated by the EMP, and the pulse has propagated out of the waveguide, they will lose their energy through collisions with neutrals or will diffuse out of the system. The plasma will then return to equilibrium T_{eo} . The electrons will thus be at a high energy for a short time, probably for considerably less than 1 microsecond.

In order to measure the energy of these hot electrons, we have built an electrostatic analyzing probe. This probe has been developed by Mix, et al.^[13], who used this device for measuring the distribution of electron energies in an electron beam. The application of their device to measuring electron energies in a plasma at energies up to 300 ev has been

developed by M. Porkolab, et al. [7]. In particular, a student of M. Porkolab has adapted this device to a machine very similar to our machine at The University of Arizona.

This device not only determines weak electron energy, but will also permit a determination of the energy distribution function. Measurement of the energy distribution function is performed on a time scale of about 5 nanoseconds. From this, number density and drift velocity should be determinable.

F. Electromagnetic Cavity and Langmuir Probes

A standard electromagnetic cavity is being used to measure ambient number density^[14]. To measure ambient electron temperature T_{eo} , we are using two Langmuir probes, one which can be moved radially into the plasma, and the other which can be moved longitudinally along the TEM waveguide. The Langmuir probe is pulsed. A voltage-current plot on an oscilloscope is obtained by applying a sawtooth voltage to the probe where the voltage is swept from zero to maximum in 3 μ s. As is well known, from the slope of this voltage-current plot, T_{eo} may be determined.

V. Description of the Equipment That Has Been Built Under Air Force Contract

A. General Layout of System

A schematic drawing of the electron-beam produced plasma system is shown in Fig. 8a. The horizontal portion of the vacuum system is about 7 feet long. A photograph of the completed machine is given in Fig. 8b.

B. Components

1. Vacuum System and External Vacuum Envelope

The vacuum envelope is of 304 stainless steel, about 8 inches OD and approximately 6 feet long. There is a 45° side port through which

emerges the output of the TEM waveguide. The vacuum system is a conventional diffusion pump backed by a fore pump. Pressures at the remote end of the chamber of order of 10^{-7} torr have been achieved.

2. Pressure Measuring System

We use a thermocouple gauge to measure air pressure down to 1 micron, and ion gauges for air pressure down to 10^{-7} torr. These gauges are used in evacuating the system initially. Nitrogen is admitted through a needle valve, and its pressure in the system is monitored by Shultz-Phelps gauges which can measure nitrogen pressure in the range 10^{-5} to 1 torr.

3. Cathode, Grid, and Collector

The cathode is a dispenser-type cathode approximately 3 inches in diameter. A grid of close spaced tungsten wires is placed about $3/4$ inch in front of the cathode. Emission of electrons from the cathode surface is controlled by the voltage difference between the grid and cathode. The resulting beam of electrons interacting with the nitrogen gas produces the plasma. The ambient number density of the plasma is controlled by the electron beam current which in turn is controlled by the grid-cathode voltage. We have found that the most stable operation can be obtained with the grid somewhat above ground. The waveguide and input conical transition serve as the collector. These elements are grounded.

4. Waveguide Assembly

The TEM waveguide parallel plates are made from stainless steel $1/4$ mesh screen welded onto a supporting track. Each plate is 7 centimeters wide, and they are separated by 3 centimeters. The waveguide is about 1 meter long with the axis at the output at 45° from the axis at the input as shown in Fig. 8. We have found that the 45° bend introduces negligible

reflections. At each end of the waveguide is a conical transition^[15]. These transitions are identical. Each is 8 inches long. A transition transforms geometrically from the TEM parallel plate waveguide to a twin-lead transmission line. The twin lead-transmission line is enclosed in a circular cylindrical stainless tube and embedded in Torr-seal^[16] (a vacuum sealing dielectric with a relative permittivity of 4.0). The twin-lead transmission thus passes through the vacuum wall. The characteristic impedance of all portions of the transmission line is 109 ohms^[17]. At both the input and output, identical tapers transform the 109 ohm twin-lead to 50 ohm coax. A cross-section of a taper is shown in Fig. 9.

5. Pulse Generator

To generate our fast rise-time, high voltage pulses, we are using a modified charged-line pulse generator, the construction of which is shown in Fig. 10. Our pulse can be characterized by three parameters: (1) rise-time, (2) fall-time, and (3) peak value. The rise-time we would like to minimize. The fall-time we would like to be able to vary. The rise-time would be minimized when we have minimized all series inductances. In embedding the switch inside the inner conductor, we have minimized the inductance.

Maximizing the peak value requires that the outer radius of the inner conductor approach the inner radius of the outer conductor since

$$V_{o(\text{peak})} = V_{in} \frac{Z_1}{Z_1 + Z_o} \quad (28)$$

where

$$Z_1 = 50 \text{ ohms}$$

$$Z_o = 42.5 \ln b/a$$

b = inner radius of outer conductor

a = outer radius of inner conductor

If we were to do this, the capacitance per centimeter would approach infinity.

$$C = 1.11 \ln b/a / \text{picofarad/cm} \quad (29)$$

The fall-time is directly related to the length and diameter of the inner conductor:

$$\text{Fall-time} = 2.2 \cdot R \cdot C$$

$$R = Z_1 + Z_o$$

$$C = 1.11 \ln b/a / \text{picofarad/cm}$$

The minimum length of the inner conductor that we can use is approximately 1 inch, the length of the reed switch plus lead length.

With all the above in mind, a 5 nanosecond fall-time pulse generator was built. This gives a maximum output voltage of 87% of the input voltage.

The measured results were as follows:

$$\text{Rise-time} \leq 160 \text{ picoseconds}$$

$$\text{Fall-time} \approx 5 \text{ nanoseconds}$$

$$V_{\text{out}} \approx 80\% V_{\text{in}}$$

The magnetic field used to operate the reed switch was obtained by winding approximately 150 turns of wire around the pulse generator and then applying a voltage to the coil. The maximum operating frequency of the reed switch is about 200 Hz.

6. Magnets

Seven magnets surround the system as may be seen in Fig. 8. In addition, a mirror magnet surrounds the input taper. The function of this latter magnet is to reflect electrons which enter the V-shaped region of the conical transition. Since an electron travelling toward the cathode will be reflected in the region between the grid and cathode, electrons will tend to be trapped longitudinally, i.e., they will be reflected at the two ends.

The current in each of the eight magnets is adjustable by means of potentiometers. We have a computer code which tells us how to set the current in each magnet for any desired magnetic field variation on the axis of the vacuum chamber.

C. Discharge Plasma System (Not constructed as of Jan. 15, 1975)

The discharge plasma system is shown schematically in Fig. 11. A glass tube, shown in Fig. 12, rectangular in cross section at one end and circular at the other is mounted in the vacuum chamber. In place of the screen TEM waveguide, two plates, made from 0.050 inch thick stainless sheet, with identical dimensions to the screen TEM waveguide (7 cm. wide, 3 cm. apart, and the same longitudinal dimensions) are screwed to the top and bottom external surfaces of the glass pyrex tube. All other parts of the transmission line system are interchangeable with the screen TEM waveguide, e.g., conical transitions, twin-lead line, and external tapers to coax.

The 3 inch cathode is replaced by a smaller 1 inch cathode which protrudes into the round portion of the glass tube. This may be seen in Fig. 11.

An arc discharge can be obtained between the cathode and the input conical transition which now acts as an anode for the discharge. We have mocked up this system, and have verified that it will work.

D. Diagnostics

1. EMP Propagation Analyzer

To determine what effect our plasma will have on the EMP, we will use the system shown in Fig. 13. The switching circuit produces a high voltage fast rise-time pulse with an exponential decay as discussed above. The pulse is then split by a power divider enabling us to view the signal before it has entered the plasma system. Since sampling scopes typically take 120 nanoseconds to respond to a trigger signal, we required a 120 nanosecond delay line between the pulse and the vertical input of the oscilloscope. The pulse propagating through the plasma will also require a delay line of 120 nanoseconds before going into the vertical input of the oscilloscope. We now have a trace of the input to the plasma and a trace of the pulse after it has been propagated by the plasma.

2. Electrostatic Analyzer Probe

The Electrostatic Analyzer Probe has as its function to measure the electron distribution function. It will certainly allow detection of 100 ev electrons. Under our present design, we can measure the distribution function either at the time the pulse passes through the waveguide or 100 or 200 picoseconds later. The probe is longitudinally movable, so that the distribution function as a function of longitudinal distance can be obtained, if desired. It can be used with either plasma system.

Figure 14 is a schematic of how we obtain the distribution function (velocity or energy) of the plasma after it has been excited by the pulse. Power supply A provides an electric field such that ions are excluded from the electrostatic probe. By varying power supply B, we obtain the integral of the electron distribution function. This is because supply B sets up an

electric field in the analyzer that repels electrons with energies lower than the supply voltage. Therefore, the number of electrons reaching the collector is directly proportional to the supply voltage. The audio oscillator and lock-in amplifier serve as a means of differentiating the collector current, thereby giving us the distribution function.

3. Electromagnetic Cavity

The Electromagnetic Cavity allows the measurement of ambient average electron number density in the plasma column^[14]. It is designed to be compatible with either plasma system. In the magnetically confined plasma, it is longitudinally movable when there is no waveguide in the vacuum system, and it will be used in this mode to initially determine longitudinal number density variations. With the waveguide in place, it remains fixed near the cathode and so can measure electron density at only that longitudinal position. It can measure ambient number densities as low as $10^7/\text{cm}^3$. In order to determine that we have number densities in the range of $10^6/\text{cm}^3$, we will have to extrapolate our cathode current and voltage data from the region of $10^7/\text{cm}^3$ and above.

We use the microwave cavity to obtain an average number density of the plasma column. Basically, we measure the resonant frequency shift of the TM_{010} mode (lowest cutoff frequency) when a plasma is present. This frequency shift, Δf , is related to the plasma frequency f_p by:

$$f_p^2 = M \Delta f f (1 + v^2/f^2) \quad (30)$$

where

M is a dimensionless constant which is a function of the ratio b/a (fig. 15)

ν is the collision frequency

f is the measured resonant frequency of the cavity
with the plasma present.

For our experiment $\nu^2/f^2 \ll 1$. The experimental apparatus is shown in Fig. 16.

4. Langmuir Probe Diagnostics

The Langmuir Probe allows absolute measurement of ambient electron temperature. It also allows relative measurement of ambient number density. The probe is pulsed over a 3 microsecond interval, so "ambient" refers to that interval. Thus, if there is a slow variation of either number density or temperature compared to 3 microseconds, the Langmuir probe will be capable of measuring these quantities as a function of time. The distribution function must approximate Maxwellian (probably unlikely except in the truly ambient case) for the measurements to have meaning that we can interpret.

Since the cavity allows absolute measurement of number density at a fixed point, this piece of information can be used to convert relative number density measurement to absolute measurements. The error in doing this is unknown at the present time.

We anticipate using Langmuir probes to obtain electron temperature and relative number density. There will be two probes, as shown in Fig. 17. One probe will be used to obtain radial measurement $[n(r), T(r)]$, and can be inserted at two locations into the plasma. The other probe will be used for axial measurements over the entire length

$$[n(z), T(z)]$$

of the structure. These probes can be used with either the electron beam-produced or discharge plasma systems. Due to the presence of the magnetic

field, it will be difficult to obtain accurate number densities from these probes. However, relative density profiles can be obtained, and compared with cavity measurements to obtain absolute number densities. Further, the magnetic field anticipated should not appreciably affect temperature measurements using the probe.

Figure 18 is a schematic of our Langmuir probe instrumentation. This equipment has been built and is presently operating. We have measured number densities of 10^9 to 10^{11} elec/cm³. A larger probe will be used for diagnostics at lower number densities (10^7 to 10^8).

VI. Preliminary Results

In this section, we present results obtained from the plasma machine, as of January 15, 1975.

A. Cold Testing the Waveguide with Time Domain Reflectometer (TDR)

To determine qualitatively whether the transitions will be of beneficial help to pulse propagation, a TDR analysis was run on the system. The setup used is shown in Fig. 19a.

If, instead of the transitions we had a direct mismatch at 50 to 109 ohms, we would expect a TDR plot such as shown in Fig. 19b. If the tapers provided a perfect match, we would expect a horizontal line TDR plot. This would correspond to a reflection coefficient of 0. Since the tapers have a reflection coefficient that varies with frequency, being higher at low frequencies than high frequencies, we should be able to qualitatively predict our TDR pattern.

Since more low frequencies will be reflected than high frequencies, we would expect the steps on the TDR plot to be gradual rises rather than

sharp rises. If this is the case, then our tapers will have served their purpose. This statement will be explained later.

The TDR plot for our system is shown in Fig. 19c. As can be seen, there are small sharp reflections along with large gradual reflections. The small reflections have reflection coefficients of about 0.08 and are too small to worry about. The large gradual reflections are as predicted.

The purpose behind using the tapers was to obtain a higher voltage through the waveguide with as little effect on the rise-time of the pulse as possible. If the tapers hadn't been used, we could only have expected approximately 60% of the input pulse voltage to propagate down the waveguide, and only 60% of that, or 35% of the input pulse, propagating out of the system. This would mean that we would have approximately 24% of the input pulse being reflected back down the waveguide, which is not a very desirable situation. Since the reflection coefficient of the tapers is lower at high frequencies, and since we are using high frequency pulses, our pulse peak amplitude will be greater than if we had had a straight mismatch. The "average" reflection coefficient of each taper can be calculated. We have found that the taper allows between 70 and 80% of the pulse voltage to propagate in the waveguide.

B. Pulse Characteristics of the System without Plasma

The system configuration is shown in Fig. 20. The pulse generator output is divided, half traveling through the system while the other half is used to trigger the scope and observe the input pulse.

The rise-times of the different components are:

<u>Equipment</u>	<u>Rise-time</u>
Oscilloscope	≤ 100 picoseconds
Delay Lines	120 picoseconds
Power Dividers	≤ 25 picoseconds
Attenuators	≤ 25 picoseconds

Since we are working with pulses with rise-times close to that of the measuring equipment, we must correct for these rise-times. This is done by the following:

$$\text{Actual Rise-time} = \sqrt{(\text{measured rise-time})^2 - \sum (\text{rise-time of equipment})^2}$$

The measured rise-time of the input and output pulses was respectively 200 ps and 450 ps. Therefore, the actual worst case rise-times of the input and output pulses are respectively 160 ps and 425 ps. Assuming that the rise-time of the waveguide is very small and the rise-times of the transitions are equal, both very good approximations, we calculated the rise-times of the tapers to be 300 ps. Knowing this, the rise-time of the pulse in the waveguide is calculated to be about 340 ps.

A plot of the input and output peak voltages as a function of the voltage across the switch is shown in Fig. 21. As can be seen, the output voltage is down about 30%. This is due to the rise-time of the tapers being slower than the rise-time of the pulse. The maximum output voltage of the system shown in Fig. 21 is about 700 volts. This value could be doubled by removing the power divider at the input and connecting the pulser directly to the taper. The trigger signal could then be obtained from the output pulse. The pulse shape was found to be independent of the voltage as would be expected.

The following is a summary of the range of values we are presently able to obtain:

Input rise-times	160 picoseconds
Output rise-time	450 picoseconds
Input fall-time	variable
Output fall-time	same as input fall-time
Input voltage	0 - 2000 volts
Voltage in waveguide	(0 -1600) volts (approximate)
Output voltage	0 - 1400 volts

C. Preliminary Study of Pulse Propagation Through Plasma Filled Waveguide

We have some very preliminary results from propagating an EMP type pulse along the TEM waveguide filled with plasma. The only diagnostic which was installed was the radial Langmuir probe. This allowed only a crude measurement of ambient number density n_{eo} , which we estimated to be about $10^9/\text{cm}^3$. The ambient neutral density was $5.16 \times 10^{18}/\text{cm}^3$ corresponding to a pressure of 1.6×10^{-3} torr. In the absence of plasma, the output pulse appeared as shown in Fig. 22 a, c, and e. The peak amplitude of the output pulse is 700, 540, and 260 volts, respectively. These pulses should be very nearly the pulses that appear at the input to the waveguide.

Regarding Fig. 22a in an input pulse to the waveguide, when a plasma is present, the corresponding output appears as in b. Similarly, for input pulses c and e, the output pulses are d and f, respectively.

In the output, initially, a ringing effect occurs with a period of 1.4 nanoseconds (ns) or a frequency of 710 MHz. If one assumes that this frequency is the plasma frequency, then n_{eo} that is predicted by this frequency is $6.3 \times 10^9/\text{cm}^3$, which is in rough agreement with the Langmuir probe estimate of n_{eo} .

During these measurements, the confining magnetic field was low enough that a further reduction of the magnetic field did not alter the results.

After about 1-1/2 periods of ringing, the output pulse amplitude increased for about 5 ns and thereafter went slowly to zero after about an additional 10 ns. The reason for this behavior is unknown.

VII. Recommendations for Future Work

By the end of the technical phase of this work (January 15, 1975), the machine itself had been completed. The diagnostic subsystems had also been completed, with the exception of the electrostatic analyzer probe, but none, except the radial Langmuir probe, had been introduced into the machine. Thus, the problems of verifying that these subsystems will do their job and work harmoniously with each other still remain to be worked out. In addition, some preliminary data have been taken, although certainly not enough to shed much light on the validity of the AFWL theory.

We present here our recommendations for the directions that this project should take, should continued funding become available. Specifically, we would recommend the following:

1. We should introduce the various diagnostic subsystems (electrostatic analyzer probe, cavity, Langmuir probes) into the plasma machine, and test each subsystem. Each must work in concert with the rest. There will be some time required to optimize the entire system. For example, at the present time, we have poor control over nitrogen gas pressure because of the high pumping speed of the diffusion pump. We anticipate that this can be overcome by a baffle that can be placed near the cathode.

2. Construct the discharge plasma. The only component missing at the present time is the pyrex tube shown in Fig. 12. We have a bid on this item indicating that its fabrication will cost approximately \$500. All other parts are on hand. This system has been designed to be compatible with all diagnostic subsystems. Some optimization will be required.

3. The complete plasma machine should then be used to obtain extensive experimental data on the effect of plasma on the propagation of an EMP through a plasma, as well as the effect of the pulse on the plasma.

Specifically, the following quantities should be measured as a function of the independent variables listed below. These quantities are: maximum energy of electrons, $T_{e\max}$, which should be measured as a function of longitudinal position; distribution function, $f(T_e)$, to be measured at discrete longitudinal points; output electric field from the TEM transmission line, $E(t)$, to be measured in real time using a sampling scope. The independent variables are: a) input EMP pulse maximum amplitude, E_0 , b) EMP input pulse rise-time, t_r ; c) the input pulse fall-time, t_f ; d) ambient number density, n_{e0} ; e) electron neutral collision frequency ν . The independent parameters should be chosen such that an incremental distance in the D-region can be simulated.

4. We should make a careful measurement of T_{e0} with the Langmuir probe. It is expected that this will be close to 1 ev. Using this value of T_{e0} , we need to have a computer run made with T_{e0} set equal to this value. The run should be made for one distance increment, and ω_p , E_0 , t_r , t_f , and ν chosen such that the scaled values are attainable in our laboratory system and the theoretically predicted results show electron temperatures approaching 100 ev. The results from this run can easily be scaled to predict the

experimental results for a range of ω_p in our laboratory plasma, where the scaling is to be done according to (27).

5. In order to understand the discrepancies between theoretical and experimental $E(t)$, a computer code should be obtained which will Fourier transform $E(t)$ into the frequency domain $E(\omega)$. Thus, for example, if discrete frequency components are dissimilar, this dissimilarity will be quickly and quantitatively perceived.

6. E_0 may have a significant effect on $f(w)$ and $T_{e\max}$. This should be carefully investigated.

7. The experimental system should be modified to include probes which will perform the following functions: a) measure maximum number density due to avalanching; b) measure average electric field as a function of longitudinal distance (the average electric field, according to the theory, should change nearly linearly with distance); c) measure the presence of electrostatic waves (these are not predicted by the theory but may be excited by the pulse).

8. Summarize the correspondence between theory and experimental data.

REFERENCES

1. Seidler, W. A., "Pulsed Power Heating of the D-region", Proceedings of the 1975 Symposium of the Effect of the Ionosphere on Space Systems and Communications, paper 3-7, Naval Research Laboratory, January 20, 1975.
2. Karzas, W. J., and R. Latter, "Detection of the Electromagnetic Radiation from Nuclear Explosions in Space", Phys. Rev. 129, B1369, (3 March) 1965.
3. Ramo, S., J. R. Whinnery, and T. Van Duzer, Fields and Waves in Communication Electronics. John Wiley and Sons, Inc., New York, 1965, p. 375.
4. Carlile, R. N., "Nonlinear Instability of Bernstein Modes Pumped by an Electromagnetic Wave", Phys. Flu. 15, 1803, (Oct.) 1972.
5. Carlile, R. N., "Wave-wave Coupling of Electrostatic Modes and an Electromagnetic Wave", Bull. Am. Phys. Soc. 16, 1274, (Nov.) 1972.
6. Jackson, E. A. "Parametric Effects of Radiation on a Plasma", Phys. Rev. 153, 235, (5 January) 1965.
7. Prokolab, M., V. Arunasalam, and R. A. Ellis, "Parametric Instability and Anomalous Heating Due to Electromagnetic Waves in Plasma" Phys. Rev. Letters 29, 1438, (20 November) 1972.
8. Forslund, D. W., J. M. Kindel, and E. L. Lindeman, "Parametric Instabilities of Electromagnetic Waves", Phys. Rev. Letters 29, 249 (1972).
9. Hall, T. A., "Observation of a High Frequency Electrostatic Wave Instability", Plasma Physics 14, 677, (July) 1972.
10. Bollinger, D., D. Boyd, H. Liu, and M. Seidl, "Production of Quiescent Plasmas in a Magnetic Field by a Beam-Plasma Discharge", Phys. Rev. Letters 28, 723 (20 March) 1972.
11. Private Communication, R. F. Ellis, Los Alamos Scientific Laboratory.
12. Private Communication, R. P. H. Chang, Bell Telephone Laboratories.
13. Mix, L. P., D. W. Swain, and J. Chang, "The Use and Limitations of an Electrostatic Analyzer for Time Resolving an Electron Beam Distribution Function", Rev. of Sci. Instrum. 44, 1703, (Dec.) 1973.
14. Slater, J. C., "Microwave Electronics", Rev. Mod. Phys. 18, 441, (Oct.) 1946.

15. Baum, C. E., "The Conical Transmission Line as a Wave Launcher and Terminator for a Cylindrical Transmission Line", Sensor and Simulation Note 31.
16. Trade-name of product manufactured by Varian Associates, Palo Alto, California.
17. Baum, C. E., "Impedance and Field Distributions for Parallel Plate Transmission Line Simulators", Sensor and Simulation Note 21.

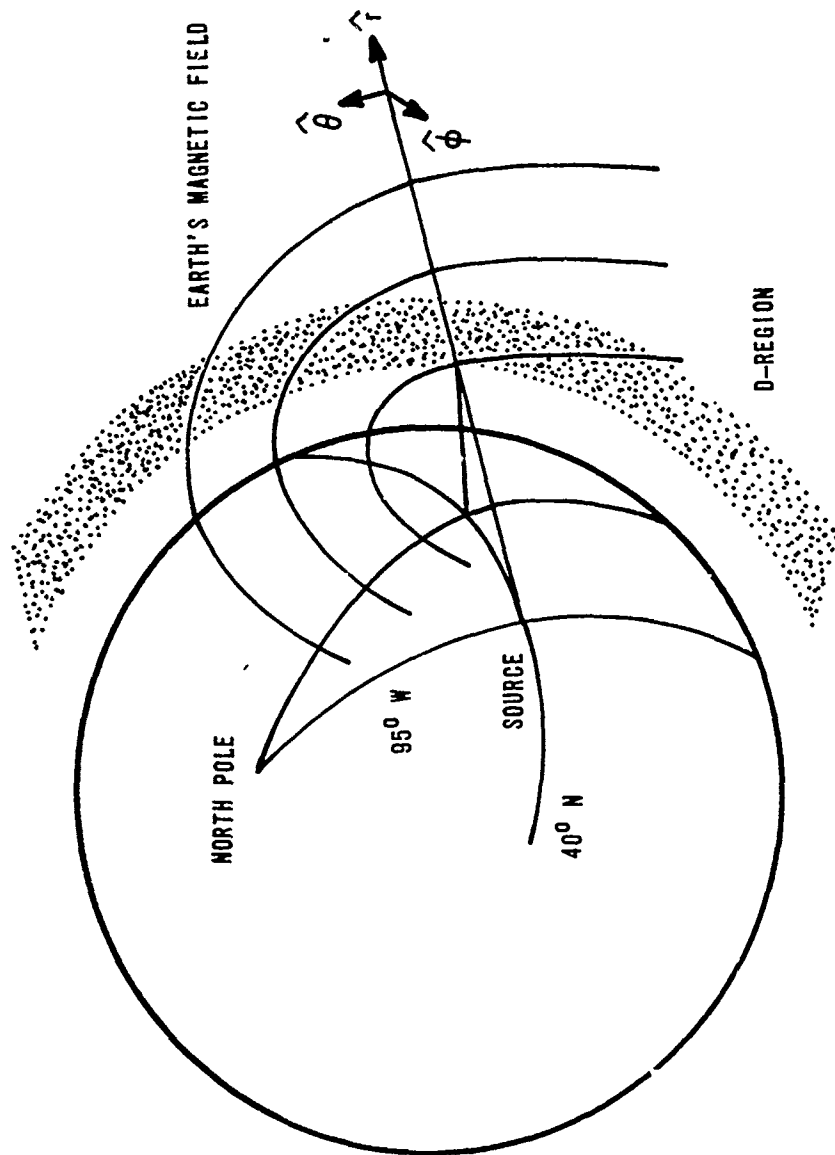


Figure 1. Geometry of one dimensional calculation of pulsed electromagnetic fields through the D-region.

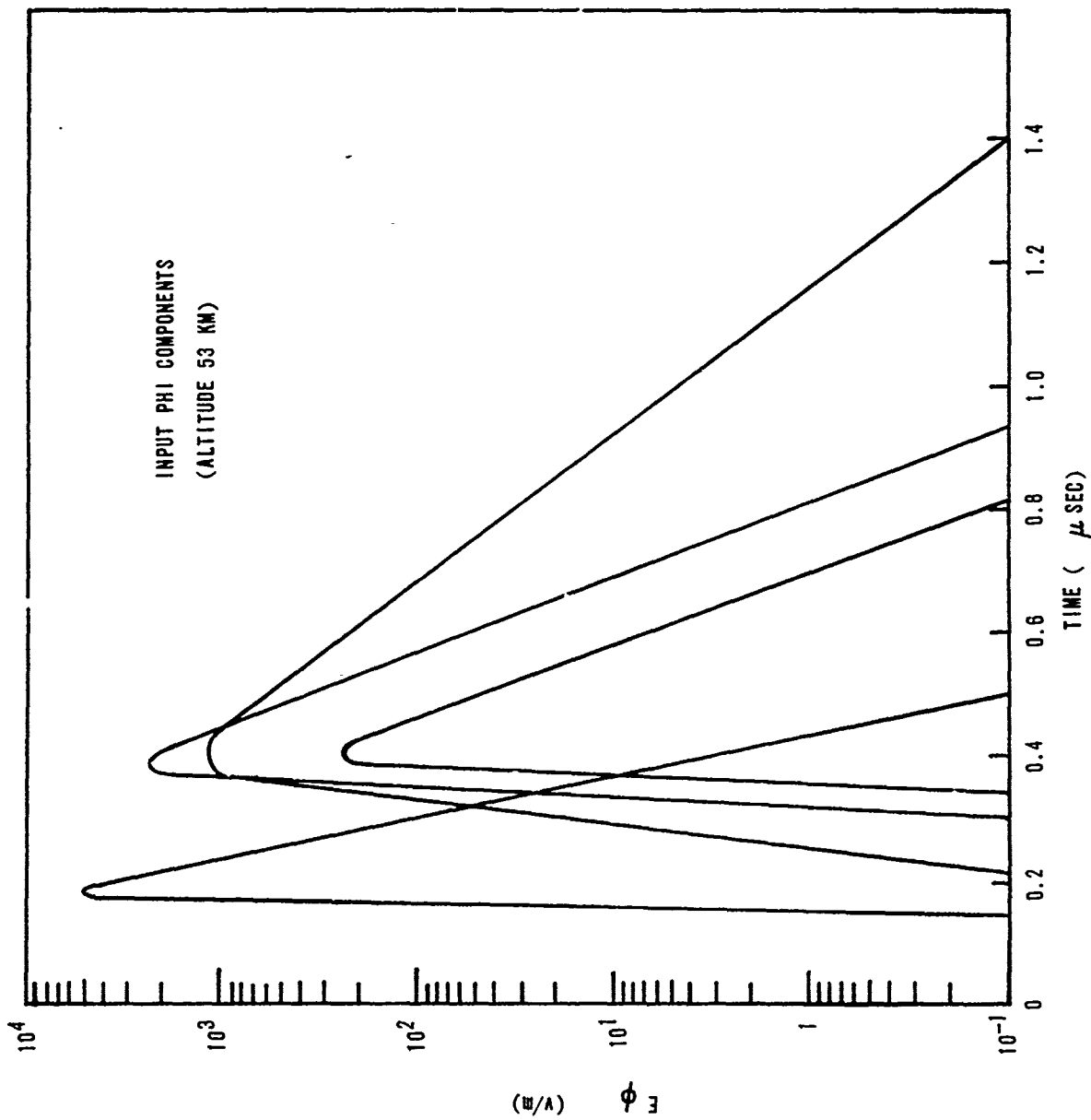


Figure 2. Electric field time histories at the entrance to the D-region.

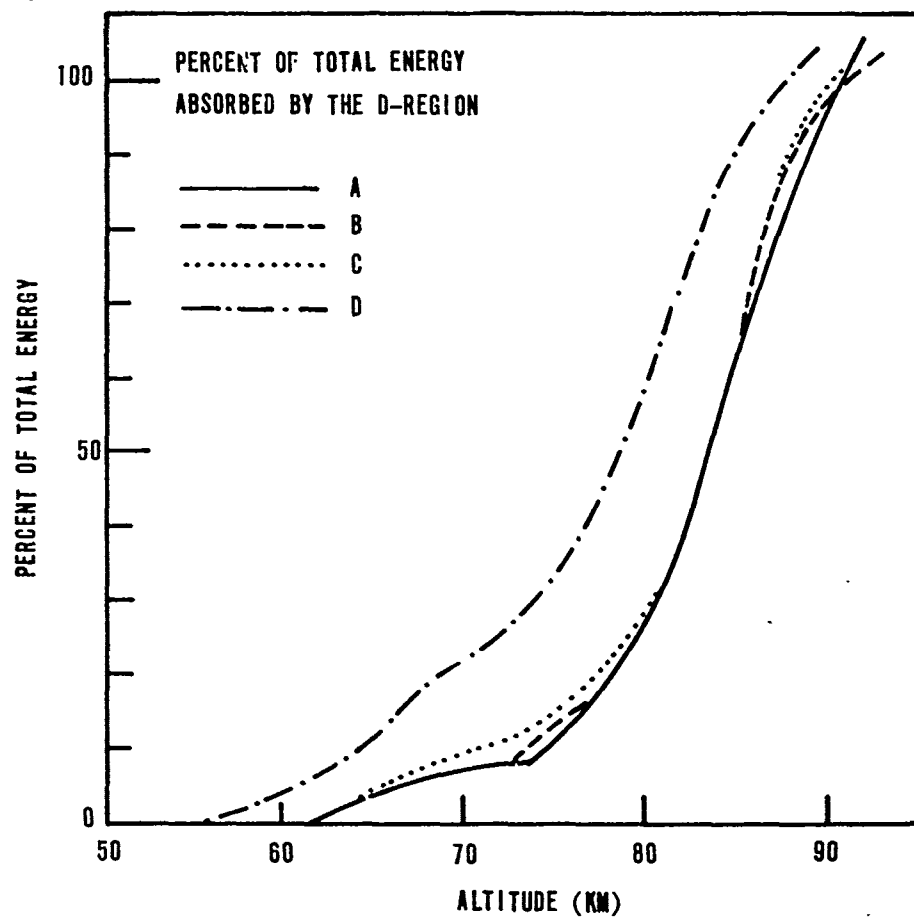


Figure 3. Energy absorption from the signal by the D-region.

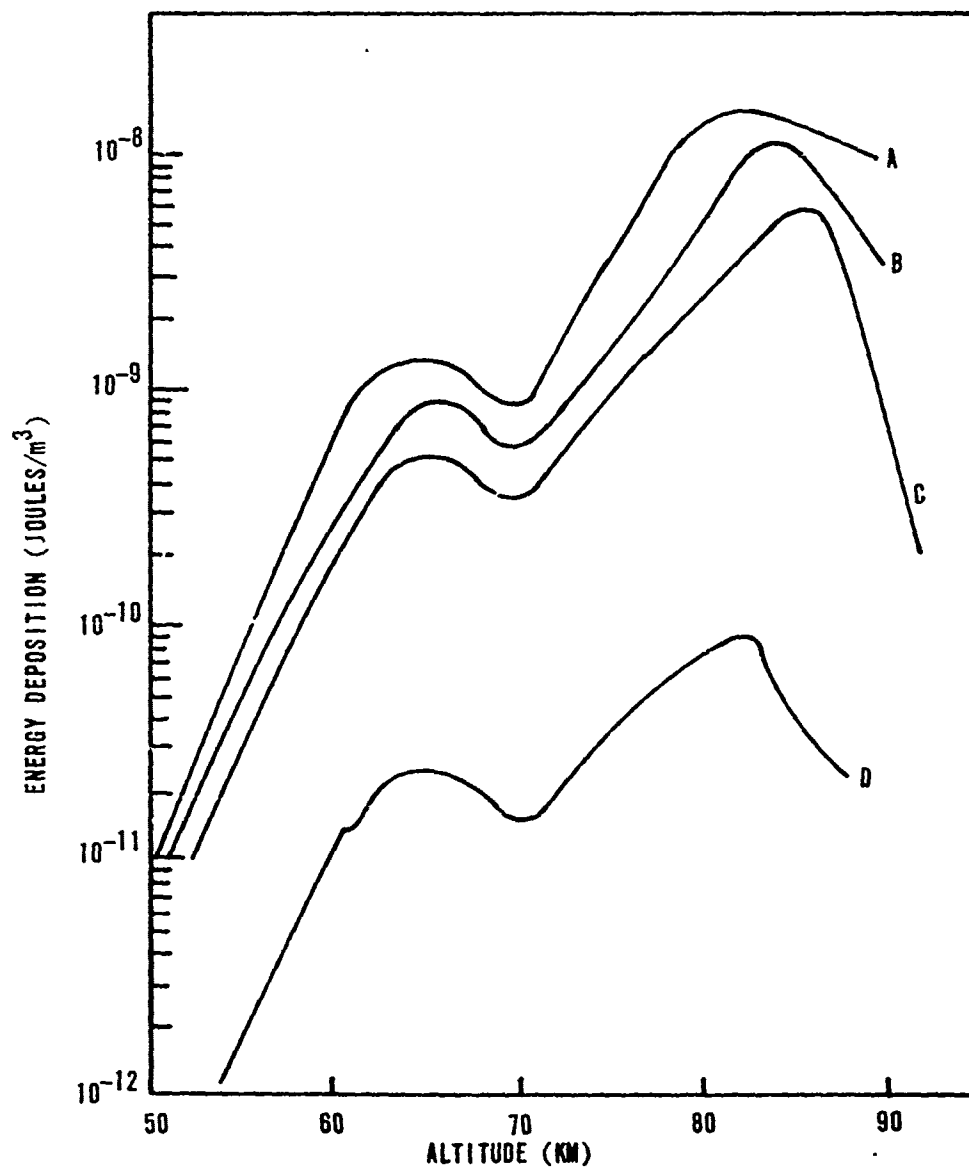


Figure 4. Energy deposition by the pulse as it tranverses the D-region.

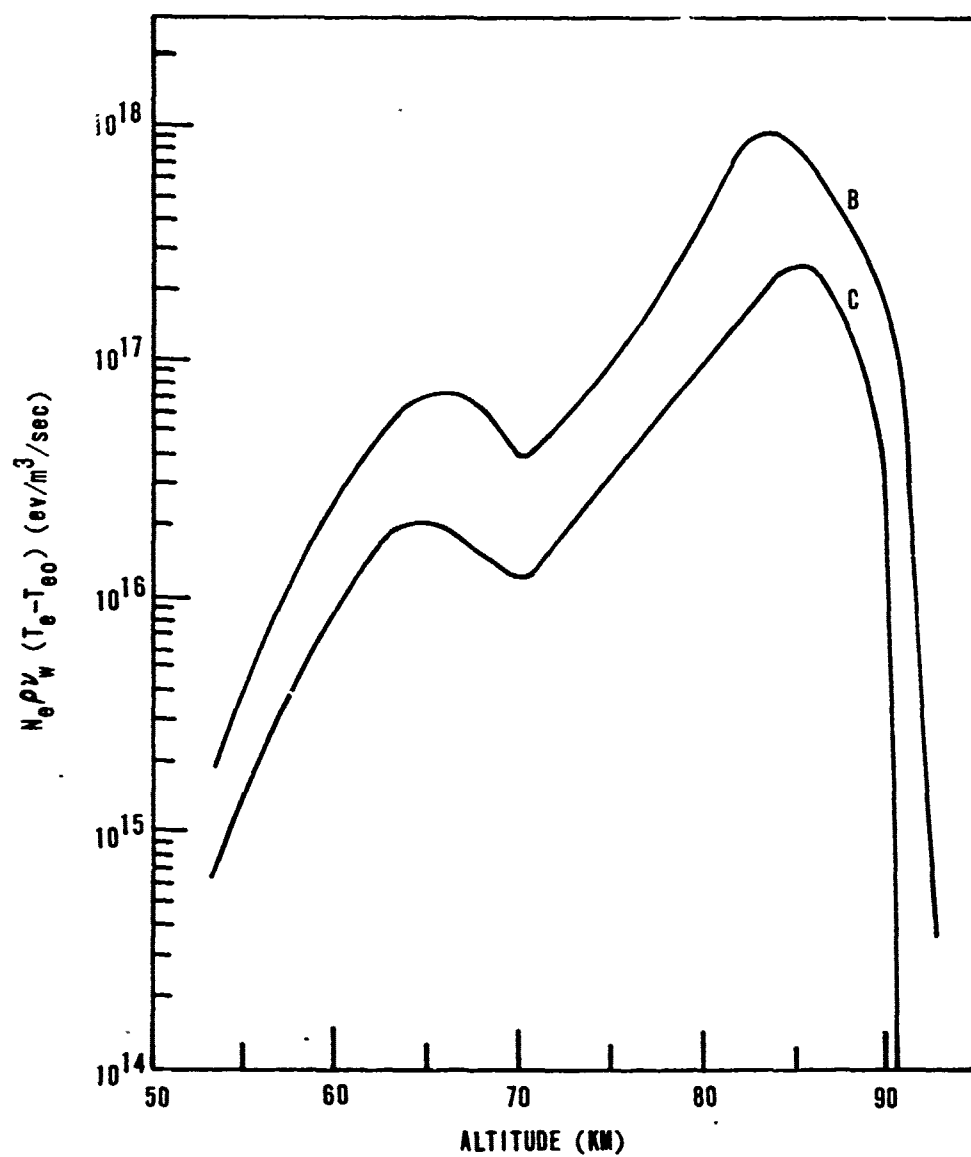


Figure 5. Energy transferred to the neutral atoms through electron neutral collisions.

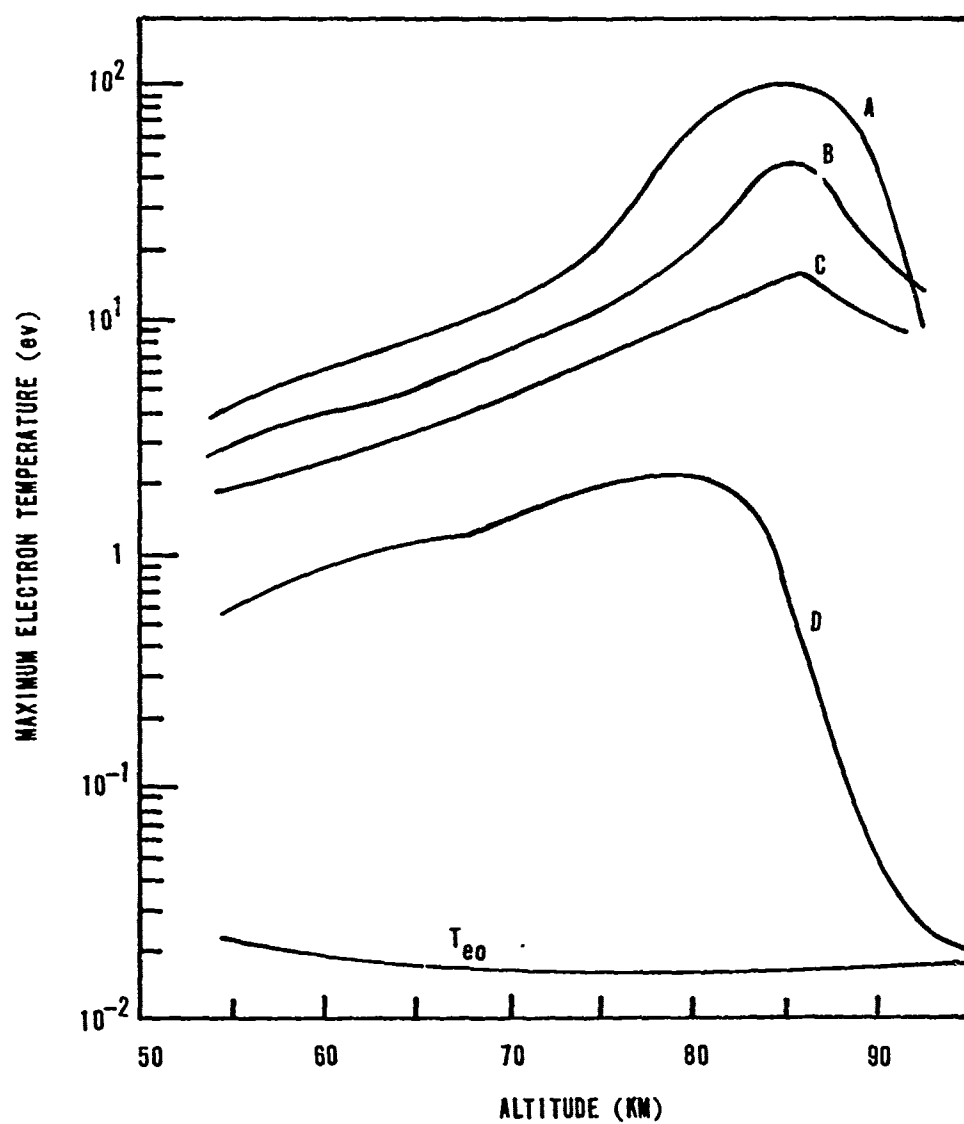


Figure 6. Maximum electron temperatures reached for pulses A, B, C and D traversing the D-region.

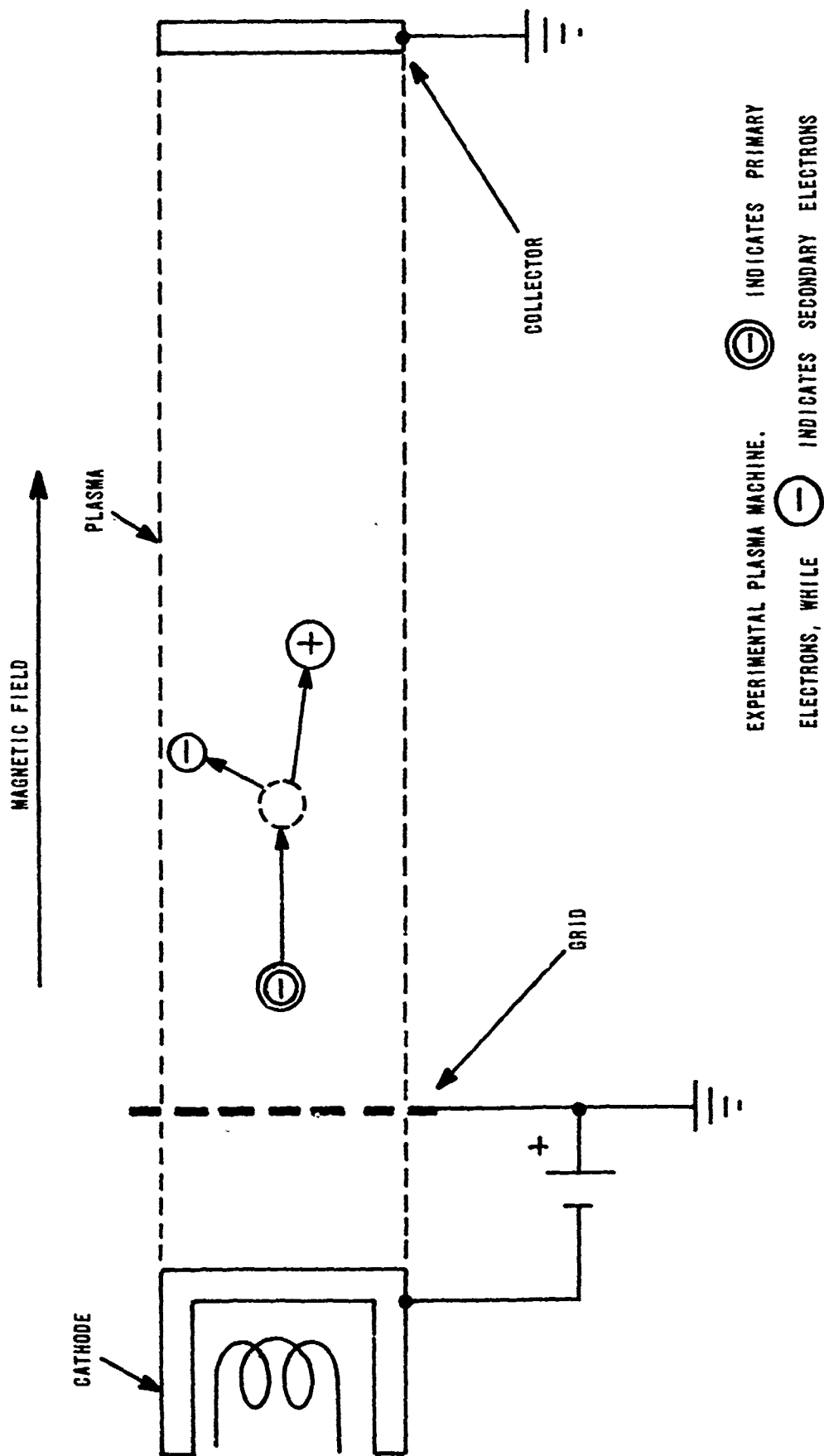


Figure 7. Schematic diagram of the beam plasma machine operation.

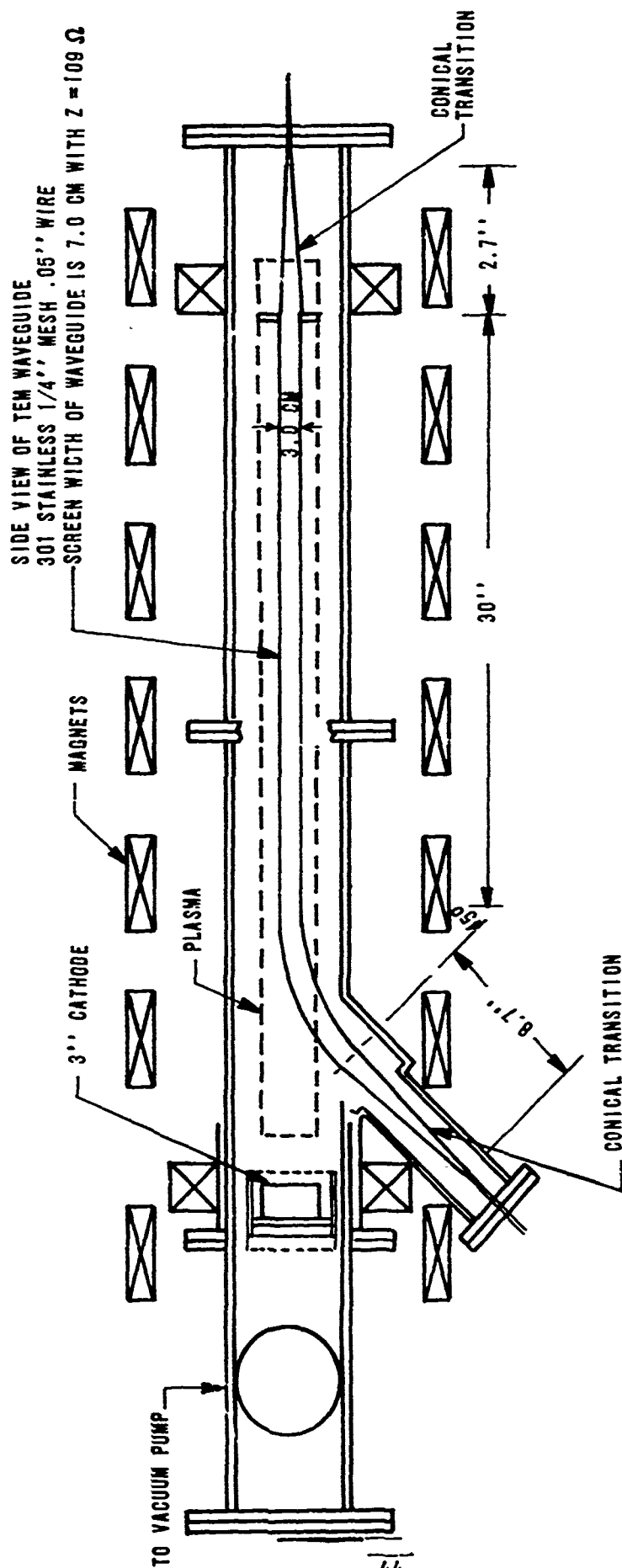


Figure 8A. A schematic of the electron-beam produced plasma system.



Figure 8B. The University of Arizona's electron-beam plasma system.

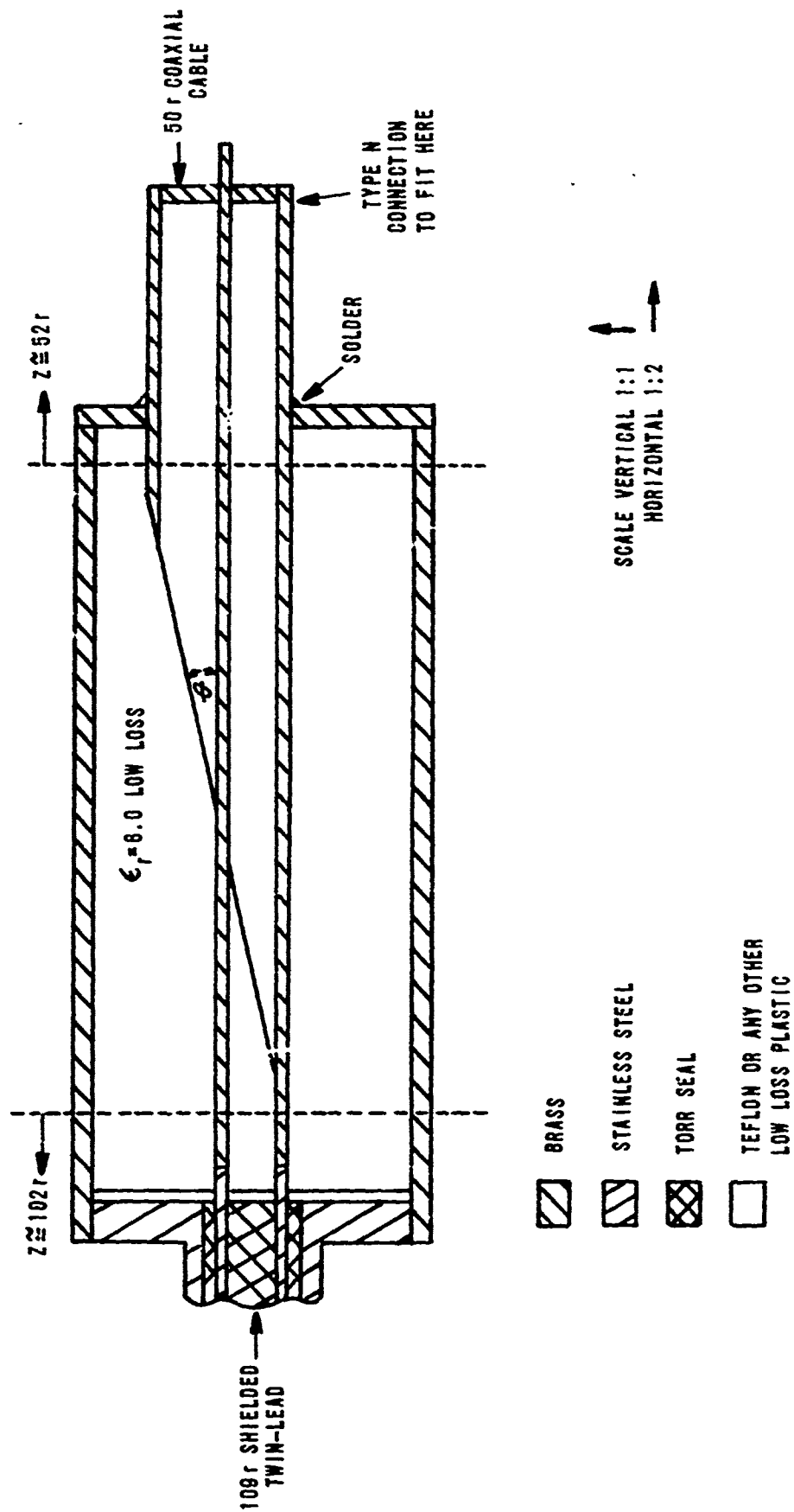


Figure 9. Impedance tapes which matches 109 ohm twin-lead to 50 ohm coax.

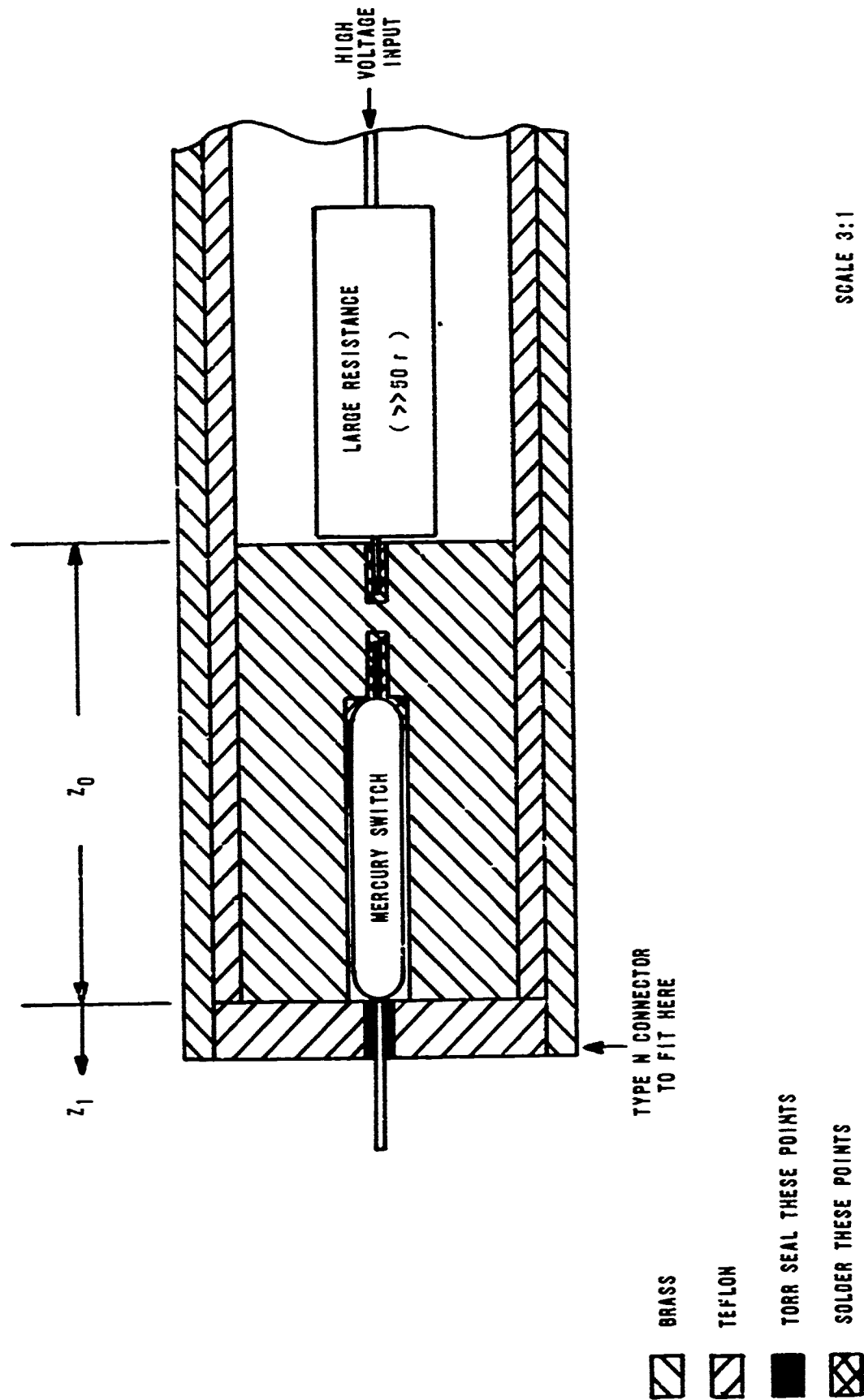


Figure 10. The modified charge-line pulse generator used to generate the fast rise-time, high voltage pulses.

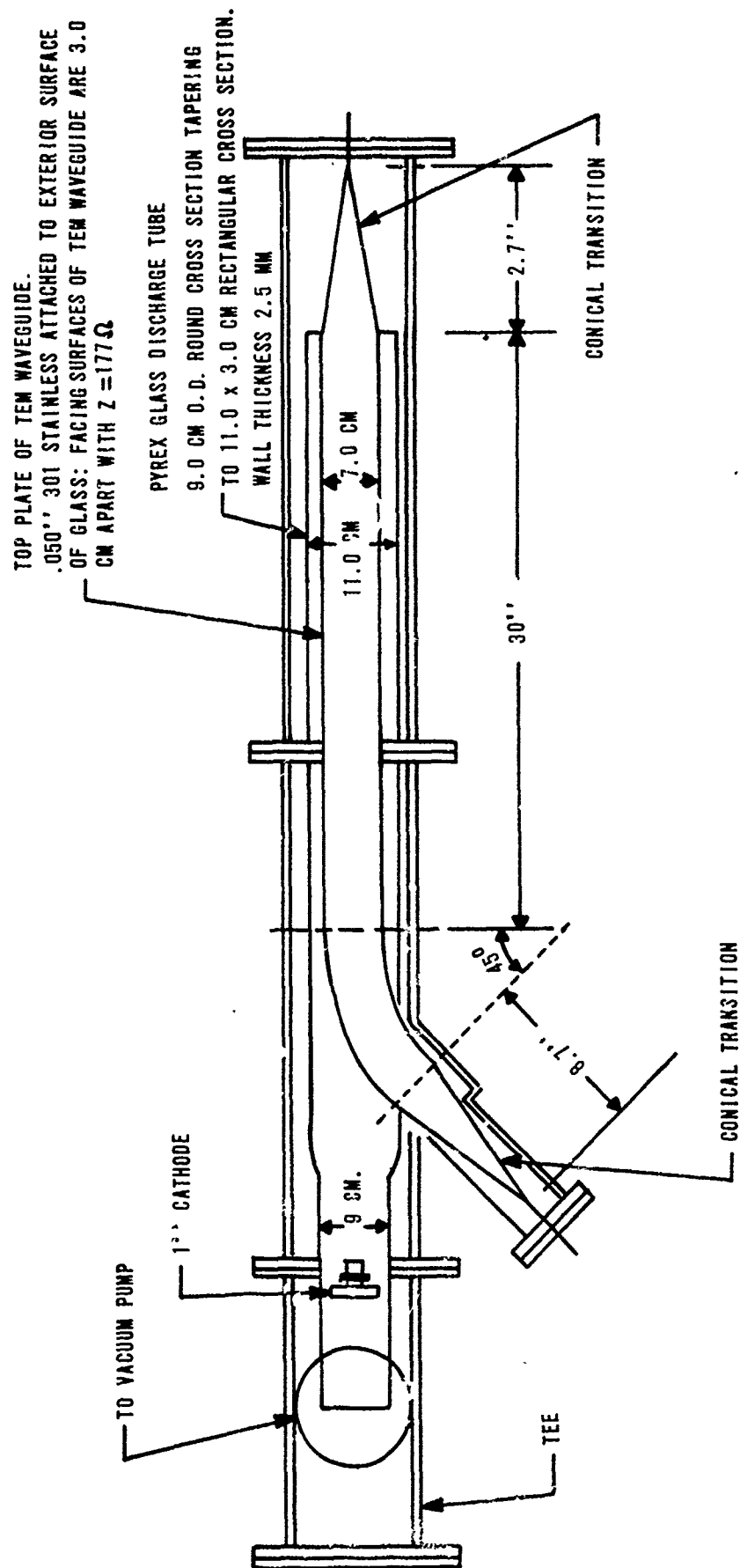


Figure 11. A schematic of the discharge plasma system.

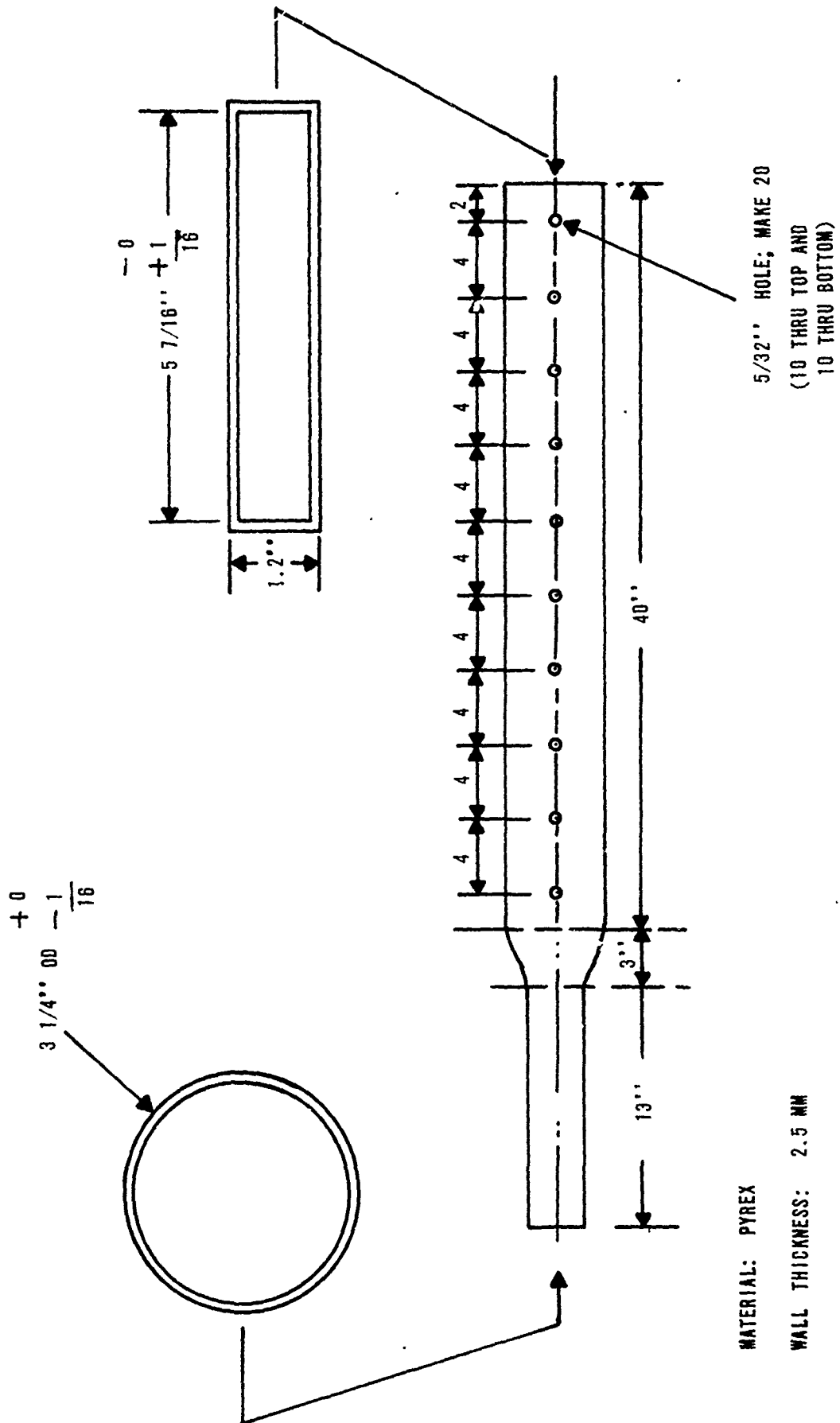


Figure 12. The glass tube used to contain the plasma in a plasma-discharge system.

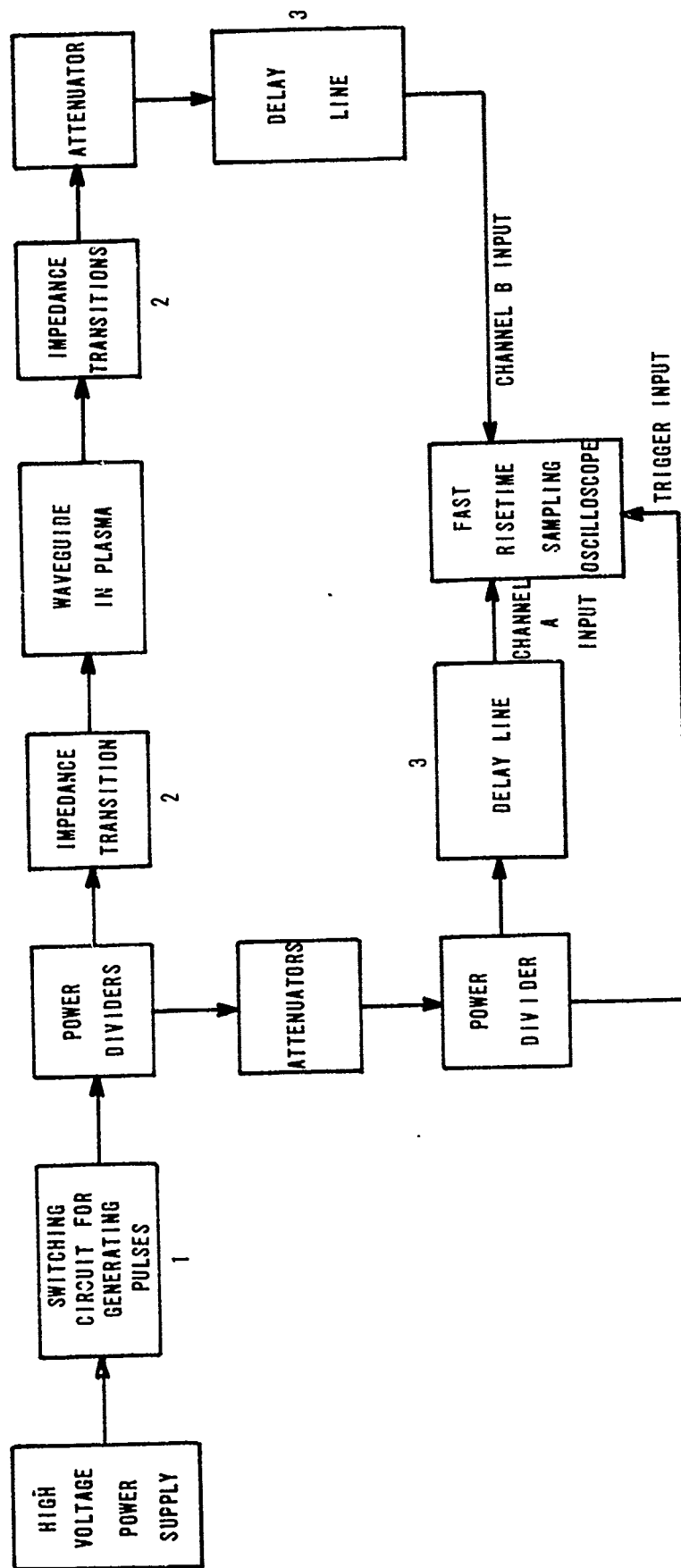


Figure 13. Schematic of the EMP propagation analyzer.

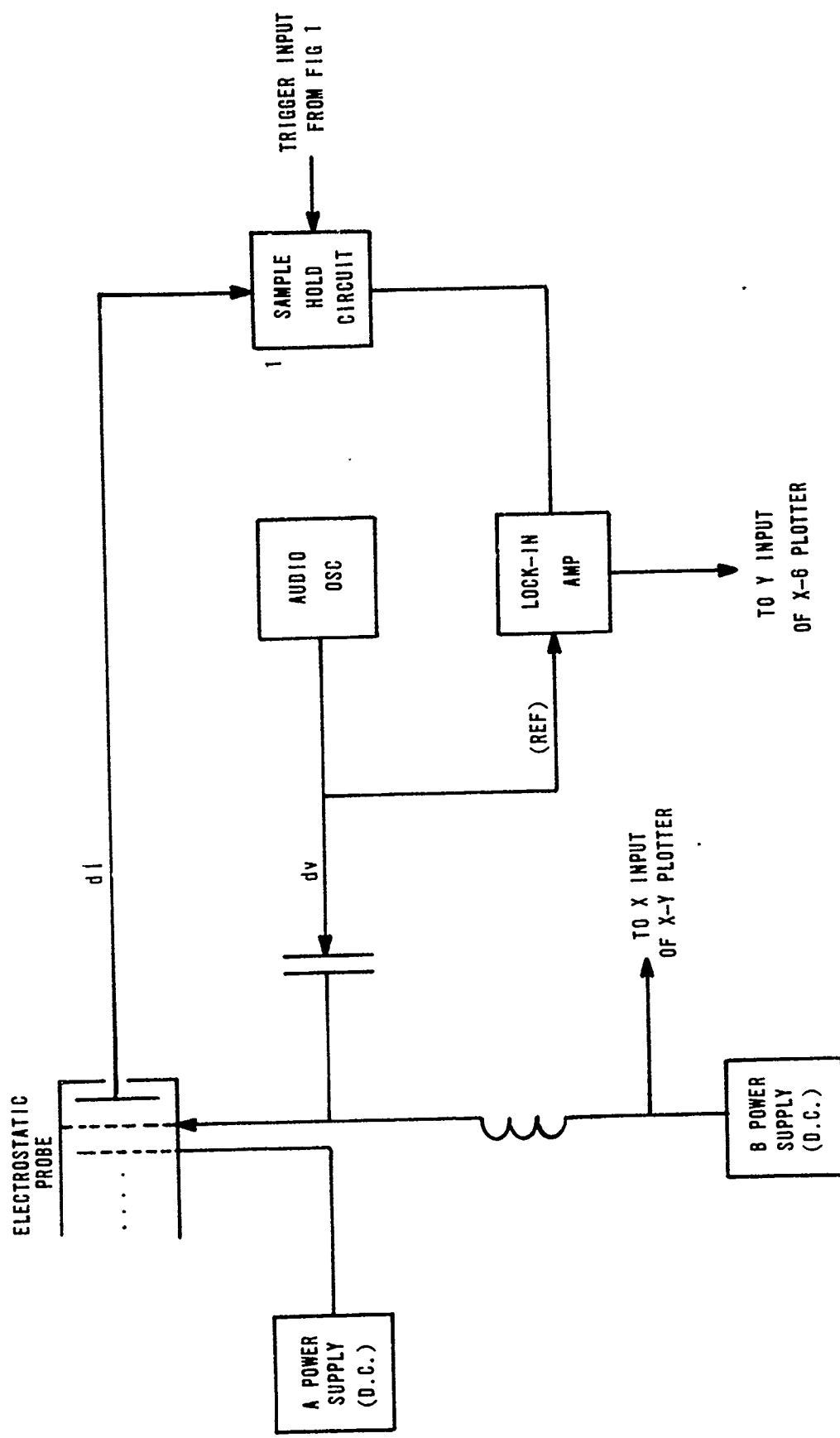


Figure 14. Schematic of system used to determine the electron distribution function.

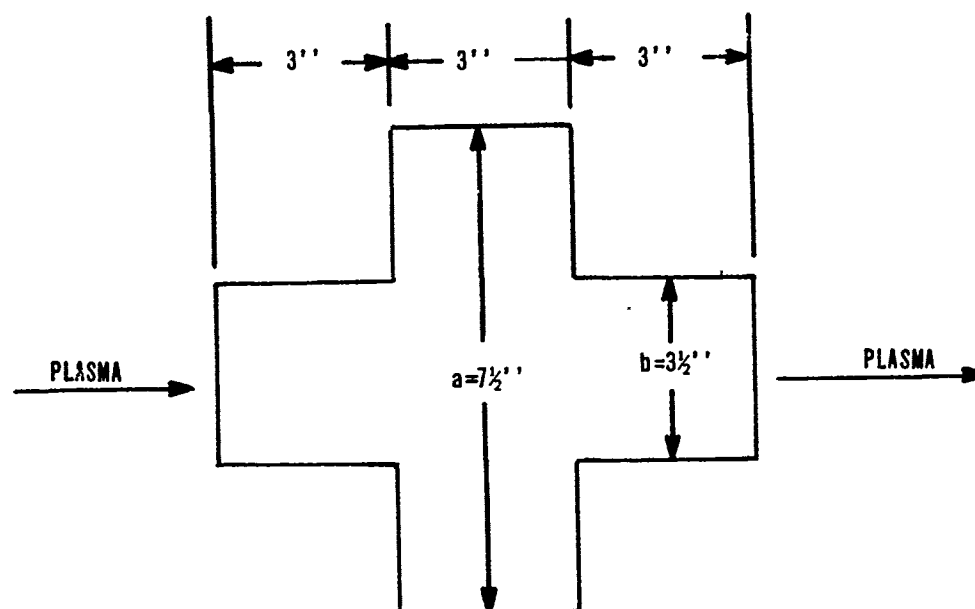


Figure 15. The electrostatic cavity used for the determination of electron number density.

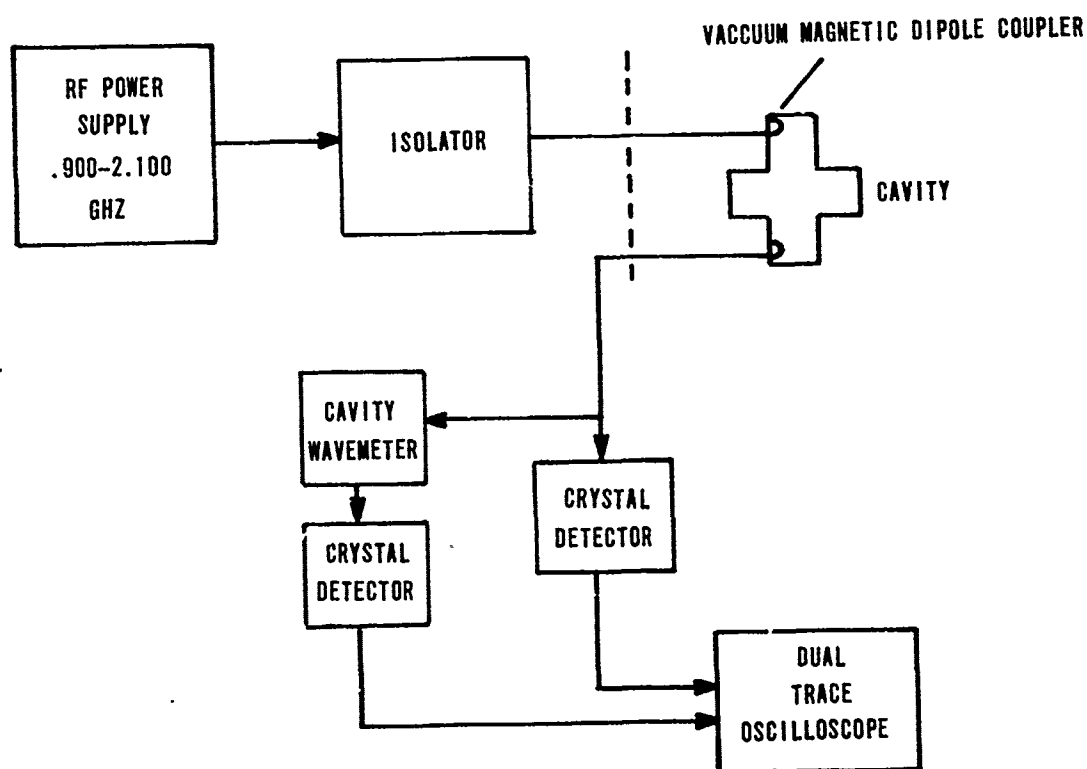


Figure 16. Schematic of the electrostatic cavity system used for the determination of electron number density.

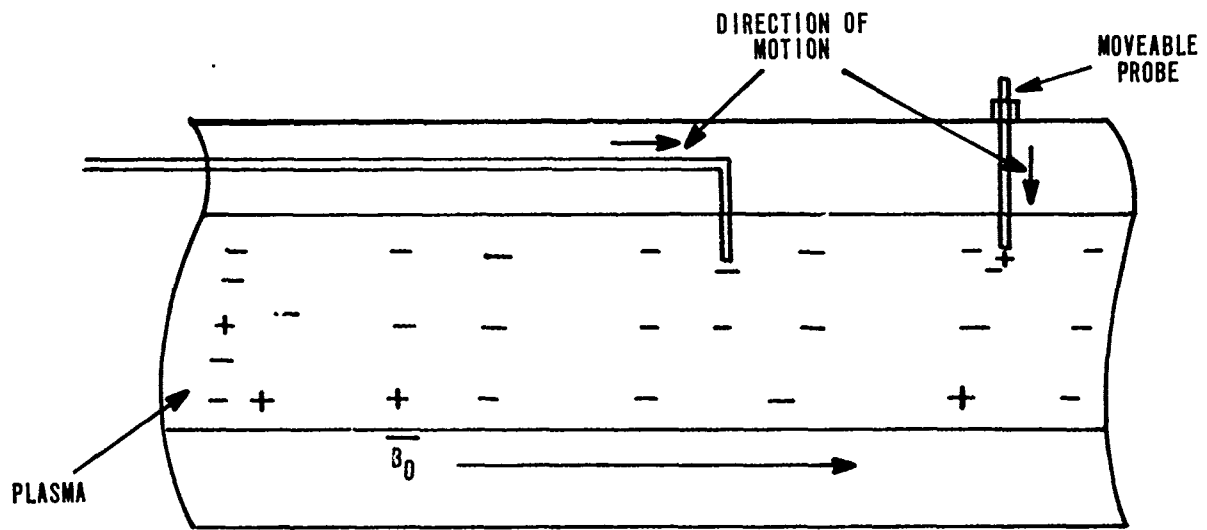


Figure 17. Diagram of the Longmire probes showing their configuration in the plasma beam.

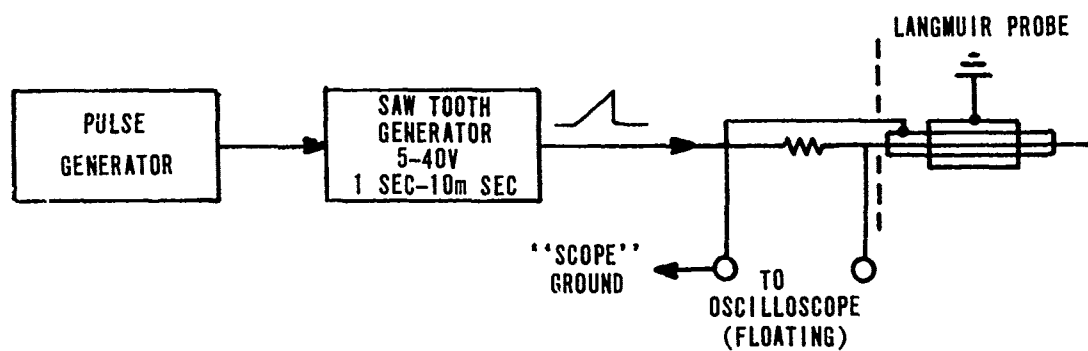
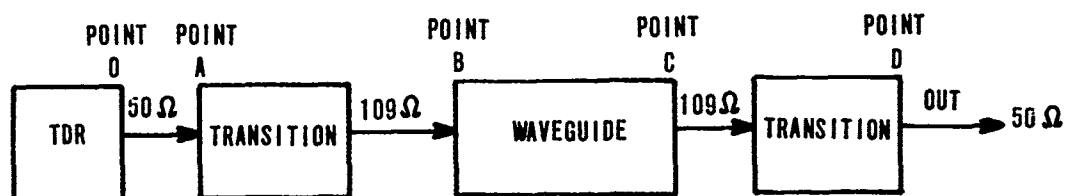
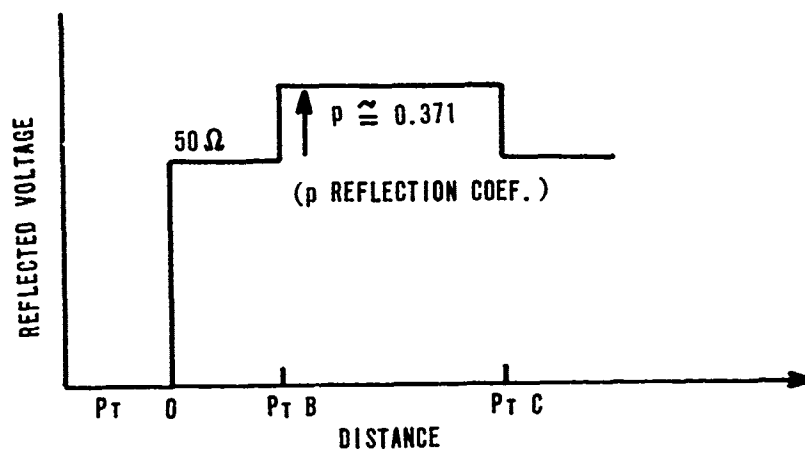


Figure 18. Schematic of the Longmire probe instrumentation.



(a)



(b)

Figure 19A. Schematic of the time domain reflectometer (TDR).

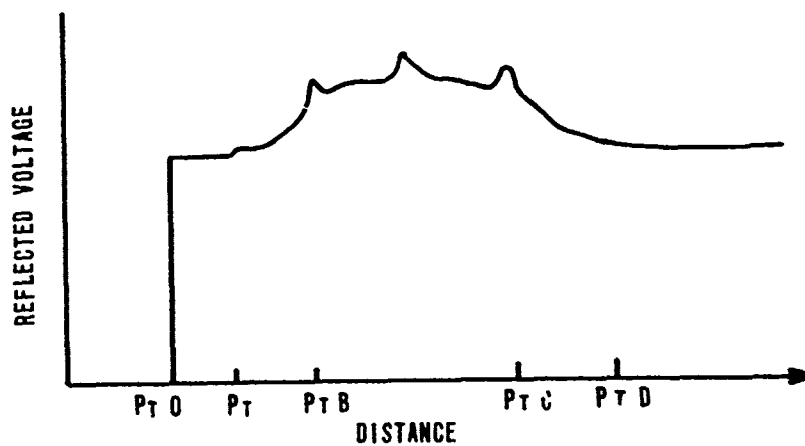


Figure 19B. Results of the TDR showing a direct mismatch at 50 ohms to 109 ohms.

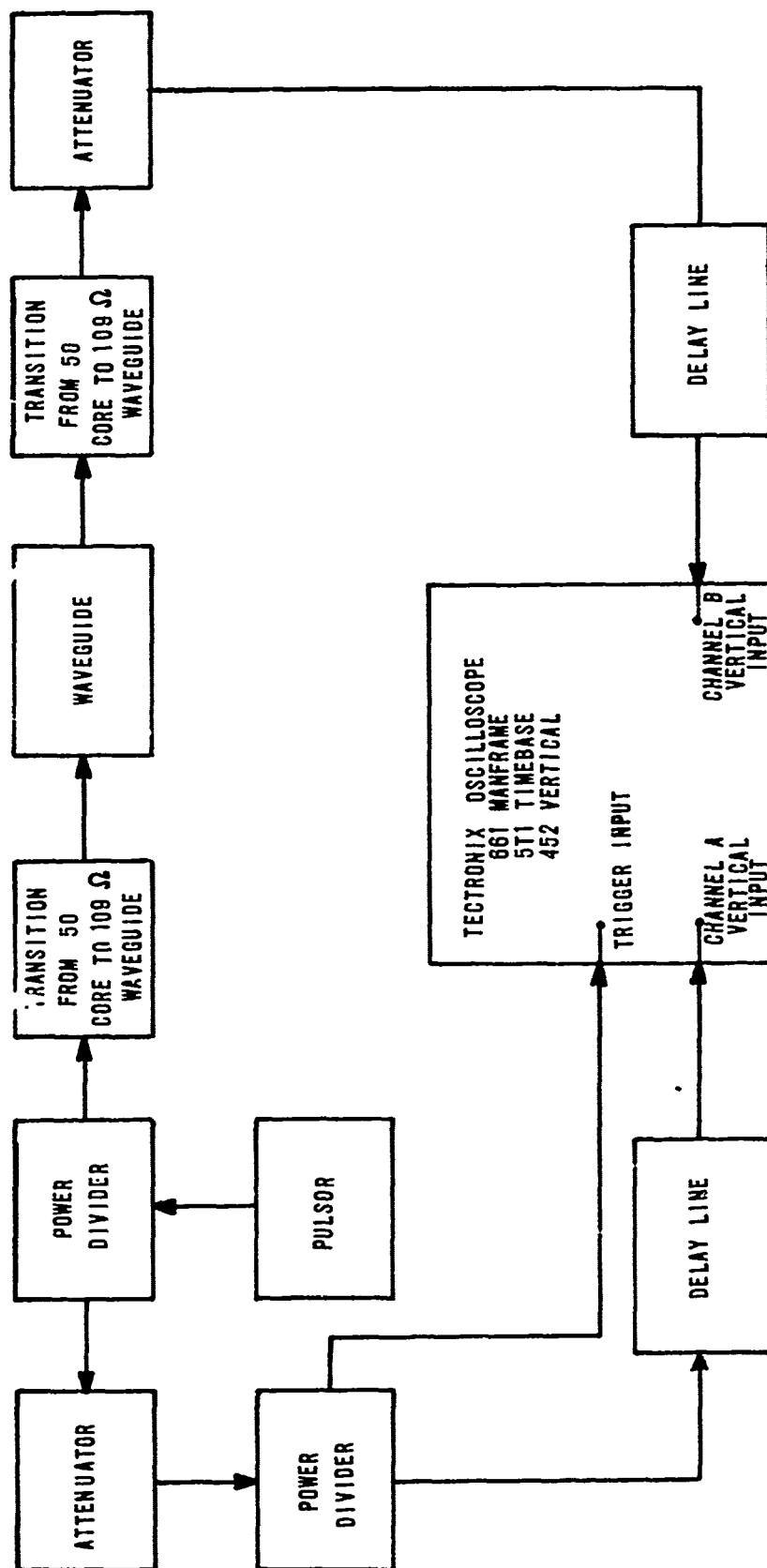


Figure 20. Schematic of EMP pulse TEM propagation line analyzing instrumentation.

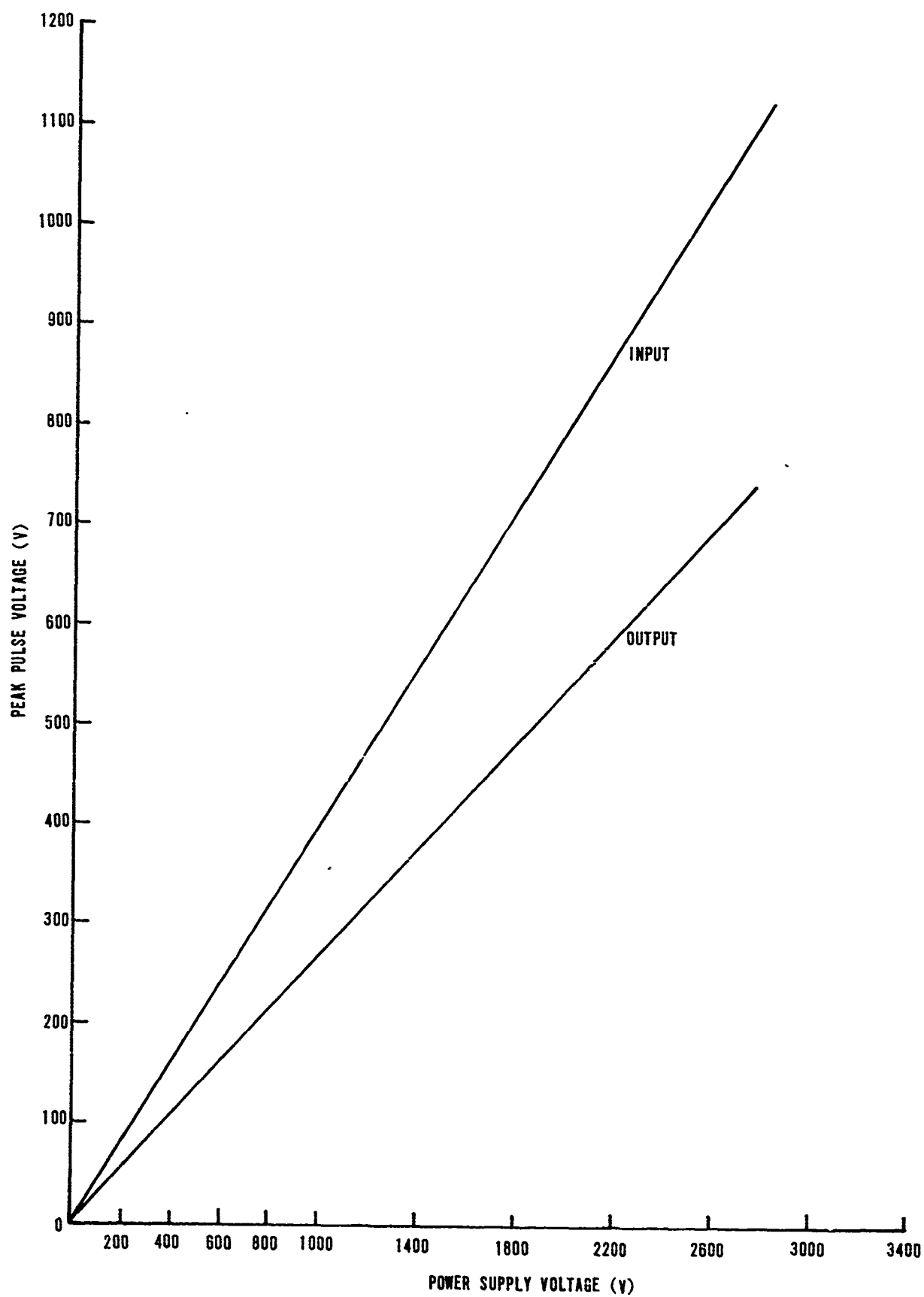
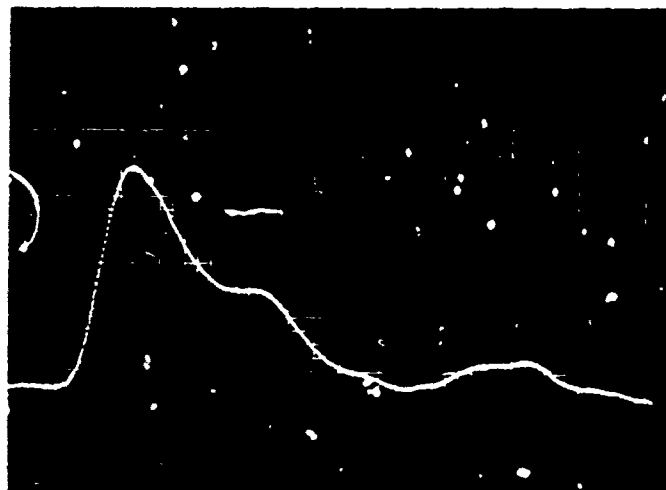
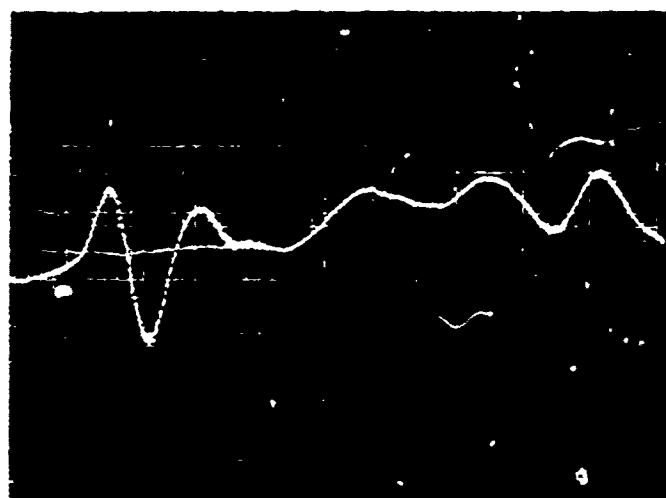


Figure 2i Input and output peak voltages as a function of voltage across the reed switch.

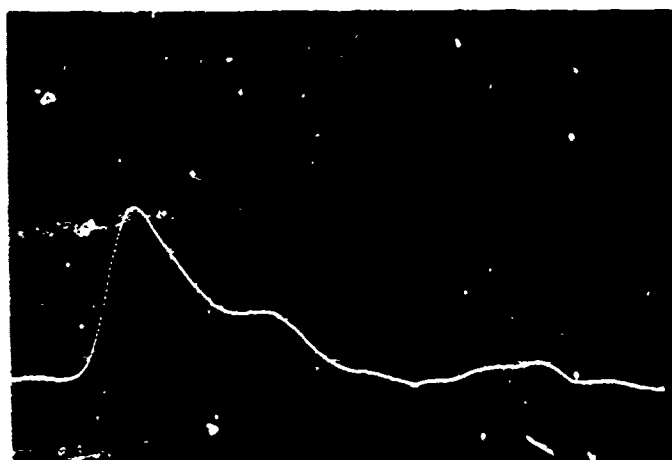


(a) INPUT PULSE; PULSE PEAK 700 VOLTS. VERTICAL SCALE, 200 V/cm.

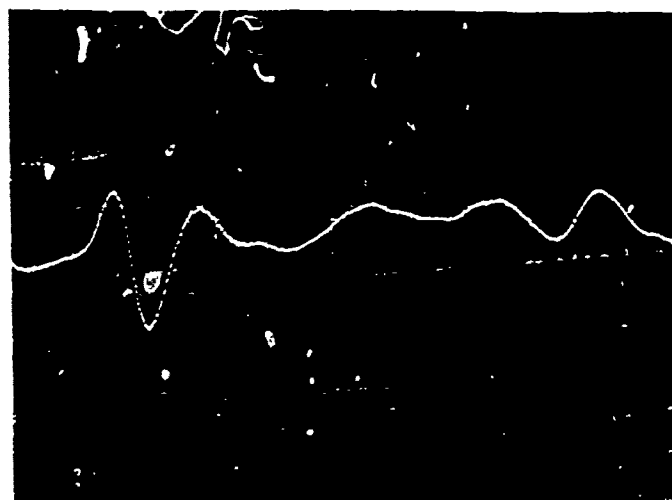


(b) OUTPUT PULSE CORRESPONDING TO (a). VERTICAL SCALE, 100 V/cm.

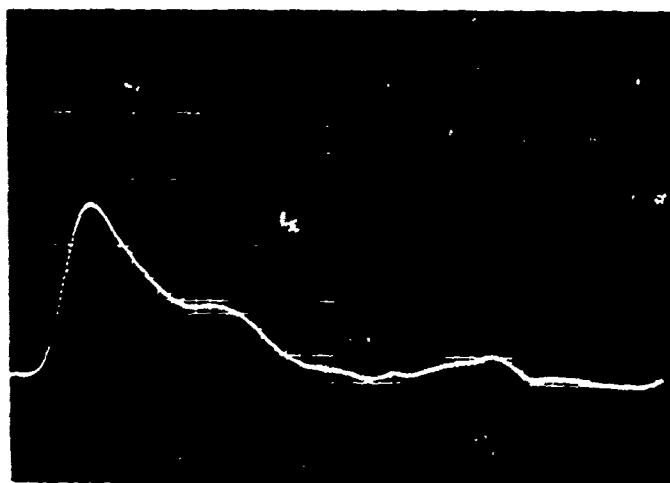
Figure 22. Input Pulses/Output Pulses



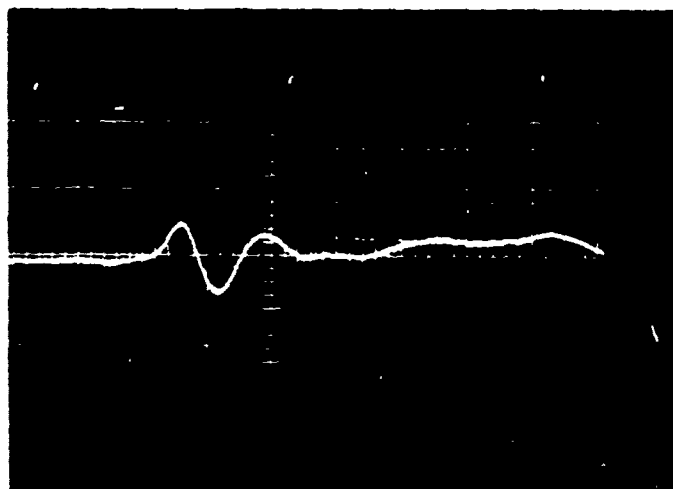
(c) INPUT PULSE; PULSE PEAK, 540 VOLTS. VERTICAL SCALE, 200 V/cm.



(d) OUTPUT PULSE CORRESPONDING TO (c). VERTICAL SCALE, 100 V/cm.



(e) INPUT PULSE; PULSE PEAK 260 VOLTS. VERTICAL SCALE, 100 V/cm.



(f) OUTPUT PULSE CORRESPONDING TO (e). VERTICAL SCALE, 100 V/cm.

DISTRIBUTION LIST

DEPARTMENT OF DEFENSE

Director
Armed Forces Radiobiology Research Institute
ATTN: R. Carter
ATTN: Commander W. Skidmore

Commander in Chief
Continental Air Defense Command JCS
ATTN: DCS/C&E, CESA

Director
Defense Civil Preparedness Agency
ATTN: TS, AED, Rm. 1C535

Defense Communication Engineer Center
ATTN: H-620, A. L. Izzo

Director
Defense Communications Agency
ATTN: Code B-210, Wpn. Sys. Anal. Div.
ATTN: Code 470
ATTN: Code H-810, J. W. McLean
ATTN: Code 346, W. H. Dix
ATTN: Code 350, J. A. Kreck
ATTN: Code 931, M. I. Burgett
ATTN: Code 350, N. A. Sica

Defense Documentation Center
2 cy ATTN: TC

Director
Defense Intelligence Agency
ATTN: DI-7D, E. O'Farrell
ATTN: DTICI, R. I. Rubinstein

Director
Defense Nuclear Agency
ATTN: DDST, P. H. Haas
ATTN: RAAE
ATTN: RAEV
ATTN: RARP
ATTN: STVL
ATTN: STSI, Archives
2 cy ATTN: STTL

Director of Defense Research & Engineering
ATTN: Dep. Dir., Strat/Sp. Sys.

Commander
Field Command, DNA
ATTN: FCTA-C

Interservice Nuclear Weapons School
ATTN: Doc. Con.

Director
Joint Strategic Target Planning Staff, JCS
ATTN: JSAS, Major Baran
ATTN: JLTW

Chief
Livermore Division, Field Command, DNA
Lawrence Livermore Laboratory
ATTN: Doc. Con. for L-395

DEPARTMENT OF DEFENSE (Continued)

National Communications Systems
Office of the Manager
ATTN: TS, D. Bodson

Director
National Security Agency
ATTN: TDL

OJCS/J-5
ATTN: J-5, P&P, R&D Div.

OJCS/J-6
ATTN: J-6, ESD-2

DEPARTMENT OF THE ARMY

U.S. Army Communications Command
CE Services Division
ATTN: CEEO-7, W. T. Heath

Chief of Research, Development & Acquisition
ATTN: LTC Edward V. DeBoeser, Jr

Department of the Army
Facils. Engrg. Support Agency
ATTN: Chief, R&T Div.

Commander
Harry Diamond Laboratories
ATTN: AMXDO-EM, Dr. J. Bombardt
ATTN: AMXDO-NP, F. Wimenitz, Chief, NWEPO
ATTN: AMXDO-RC, Dr. R. Oswald, Chief, Lab. 300

Commander
Picatinny Arsenal
ATTN: P. Harris
ATTN: A. Nichols, NDR 300, Bldg. 95

Commander
Redstone Scientific Information Center
U.S. Army Missile Command
ATTN: Chief, Doc. Sec.

President
U.S. Army Airborne Comm. & Elect. Bd.
ATTN: STEB-MA-A

Commander
U.S. Army Armor Center
ATTN: ATSAR-CD-MS

Director
U.S. Army Ballistic Research Laboratories
ATTN: AMNRD-BRD, Dr. Eccleshall

Chief
U.S. Army Communications Sys. Agency
ATTN: SCCM-AD-SV

Commander
U.S. Army Computer Systems Command
ATTN: CSCS-EME-C

DEPARTMENT OF THE ARMY (Continued)

Commander
USAEC

ATTN: AMSEL-TL-NC, Dr. W. J. Ramm

Commanding Officer
Night Vision Laboratory
USAEC

ATTN: CPT S. Parker

Commander

USA Elec. Pvg. Gnd.

ATTN: STELP-MT-M, Mr. Durbin

Division Engineer

USA Eng, Missouri River

ATTN: MRDED-MC, F. L. Hazlett, R&I Coord.

Commandant

USA Fld. Art. Sch.

ATTN: ATSFA-CT-ME, CPT Craig

Commander

USA Forces Command

ATTN: AFOP-TS

Commander

USA M/MRC

ATTN: AMXMR-HH, J. Dignam

Commander

USAMC

ATTN: AMCRD-WN, J. F. Corrigan

Commander

USANC

ATTN: AMCPM-LCES, H. Henriksen

ATTN: AMSMI-RGP, H. Green

Commander

USAMER&DC

ATTN: SNEFB-ES, R. S. Brantly

Commander

USA Nuc. Agey.

ATTN: ATCN-W

Commander

BMD Sys. Command

ATTN: SSC-TEN, N. Hurst

Chief

USA Nuc/Chem Surety Grp.

ATTN: FDSG-ND, Bldg. 2073, North Area

Commander

TRASANA

ATTN: SSEA-EAB, F. N. Winans

Commander

USASA

ATTN: IARD-T, Dr. R. H. Burkhardt

Project Manager

USA IDS, AMC

ATTN: AMCPN-TDS-TF

Commander

USA TAC

ATTN: AMCPM-GCM-SW, L. A. Wolcott

DEPARTMENT OF THE ARMY (Continued)

Commander

USAT&EC

ATTN: AMSTE-EL, R. I. Kolchin

Commander

USA T&DC

ATTN: ATOI-SD

Commander

WSMR

ATTN: STEWS-TE-NT, M. P. Squires

DEPARTMENT OF THE NAVY

Chief of Nav. Ops.

ATTN: OP-622C, R. Piacesi

Chief of Nav. Rsch.

ATTN: Code 418, Dr. T. P. Quinn

Commander

Nav. Air Sys. Command

ATTN: AIR-350-F, LCDR H. Hardt

Commanding Officer

Nav. Ammo. Dep.

ATTN: Code 7024, J. L. Ramsey

Officer-in-Charge

Nav. Constr. Bat. Ctr.

ATTN: Code L-31

Commander

Nav. Elec. Sys. Command

ATTN: ELEX 05123

Commander

NELC

ATTN: Code 3100, E. E. McCown

Commanding Officer

NISC

ATTN: NISC-41

Commander

Naval Surface Weapons Center

6 cy ATTN: Tech. Lib./Info. Svc. Div.

Commander

Nav. Ord. Sys. Command

ATTN: GRD-034C, S. Barham

Director

NRL

ATTN: Code 6633, J. C. Ritzer

ATTN: Code 7701, J. D. Brown

Commander

Nav. Ship. Eng. Ctr.

ATTN: Code 617402, E. F. Duffy

Commander

NWC

ATTN: Code 753

Commanding Officer

NWEP

ATTN: L. Oliver

DEPARTMENT OF THE NAVY (Continued)

Commander

NWL

ATTN: Code GBR, R. C. VanWagoner

Director

SSPO

ATTN: NSP-234, R. Coleman

ATTN: NSP-2431, G. W. Hoskins

ATTN: NSP-230, D. Gold

CICUSPF

ATTN: Doc. Con. 303

DEPARTMENT OF THE AIR FORCE

Commander

ASD

ATTN: YHEX, Maj R. Leverette

Commander

ADC/AD

ATTN: ADGPP-A

Commander

ADC/XP

ATTN: XPQDQ, Maj G. Kuck

ARL

ATTN: LS, Y. S. Park

AFAL

ATTN: DLOSL

Commandant

AFFDL

ATTN: R. Beavin

AFWL

ATTN: SAY

ATTN: DYX, Dr. D. C. Wunsch

ATTN: HO

ATTN: EL, J. Darrah

ATTN: ELA

ATTN: SAB

ATTN: EL

ATTN: ELC

2 cy ATTN: SUL

10 cy ATTN: ELP, Dr. W. Page

AFTAC

ATTN: TAP

ATTN: TND

ATTN: TAE

AFAL

ATTN: TEA, Dr. H. J. Hennecke

ATTN: TEA, E. C. Maupin

HQUSAF/RD

ATTN: RDQPN

ESD

ATTN: XRP, Maj Gingrich

FTD

ATTN: PDTN, Mr. Ballard

CICSAC

ATTN: XPFS, Capt Deraad

DEPARTMENT OF THE AIR FORCE (Continued)

USAF School of Applied Sciences

ATTN: TEOS-51, Capt Kaepfel

SAMSO/RS

ATTN: RSP, Lt Col Gilbert

SAMSO/SK

ATTN: SKT, P. H. Stadler

SAMSO/SZ

ATTN: SZJ, Capt DeJonckheere

SAMSO/DY

ATTN: DYS, Maj Heilman

SAMSO/IN

ATTN: IND, I. J. Judy

ENERGY RESEARCH & DEVELOPMENT ADMINISTRATION

LASL

ATTN: Dr. J. S. Malik

ATTN: P. F. Taschek

ATTN: J-8, Dr. R. Partridge

Sandia Lab.

ATTN: J. A. Mogford, Div. 8341

Sandia Lab.

ATTN: Org. 5245, T. H. Martin

ATTN: Org. 5223, C. N. Vittitoe

UCC, ORNL

ATTN: Dr. D. B. Nelson

LLL

ATTN: L. M. Erickson, L-24

ATTN: R. A. Victor, L-126

ATTN: Dr. M. W. Knapp, L-531

ATTN: Dr. W. J. Hogan, L-531

LRL

ATTN: Prof. K. M. Watson

OTHER GOVERNMENT AGENCIES

CIA

ATTN: RD/SI, Rm. 5G48, Hdq. Bldg. for
W. A. Decker

Dept. of Interior

Def. Elec. Pwr. Admin.

ATTN: Doc. Con.

FAA

Hdq. Sec. Br., ASE-210

ATTN: F. S. Sakate, PD 650

NAS

ATTN: Dr. R. S. Shane, Nat. Mat. Adv. Bd.

NASA

Marshall SFC

ATTN: ASTR-MTD, A. D. Coleman, Bldg. 4476

NASA

Lewis RC

ATTN: Library

DEPARTMENT OF DEFENSE CONTRACTORS

Aerajet Elec. Sys. Co.
Aerojet-Gen. Corp.
ATTN: T. D. Hanscome, Bldg. 170, Dept. 6711

Aerospace Corp.
ATTN: Library
ATTN: V. Josephson, Dev./Surv. Dir.

Analog Tech. Corp.
ATTN: J. J. Baum

Avco
ATTN: Research Library, A-680, Rm. 2201

Battelle Memorial Institute
ATTN: R. K. Thatcher

Bell Aerospace Corp.
ATTN: C. B. Schoch, M.S. I-85

The Bendix Corp.
Aerospace Sys. Div.
ATTN: R. H. Pizarek

The Bendix Corp.
Nav./Cont. Div.
ATTN: E. E. Lademann

The Boeing Co.
ATTN: Aerospace Library

The BDM Corp.
ATTN: J. J. Kalinowski

The BDM Corp.
ATTN: R. B. Buchanan

Brown Engineering Co.
ATTN: J. M. McSwain, M.S. 18

Brunswick Corp.
ATTN: S. Woznick

C. S. Draper Lab.
ATTN: K. Fertig

Com. Sci. Corp.
ATTN: J. D. Ilgen

Cudler-Hammer, Inc.
AIL Div.
ATTN: A. Anthony, Central Tech. Files

Dikewood Corp.
ATTN: L. W. Davis

E-Sys., Inc.
ATTN: Library, 8-51910

EG&G, Inc.
ATTN: H. H. Hoffman

Exp. & Math. Phys. Con.
ATTN: T. M. Jordan

Fairchild Camera & Instrument Corp.
ATTN: D. K. Myers, 2-233

DEPARTMENT OF DEFENSE CONTRACTORS (Continued)

Fairchild Ind., Inc.
ATTN: W. Metzger

Franklin Inst.
ATTN: R. H. Thompson

Gen. Dyn. Corp.
Elec. Div.
ATTN: R. E. Fixsen, 7-11, SED

General Electric Co.
ATTN: J. R. Greenbaum
ATTN: L. Chasen

General Electric Co.
TEMPO-Center for Advanced Studies
ATTN: DASAC, Ref. File

General Electric Co.
Aerospace Elec. Sys.
ATTN: F. Nicotera, M.S. 624

General Electric Co.
REESD
ATTN: R. V. Benedict

General Electric Co.
Ord. Sys.
ATTN: D. Corman, Mail No. 2171

General Electric Co.
AEG-Tech. Info. Ctr.
ATTN: J. A. Ellerhorst, E-2

General Research Corp.
ATTN: P. J. Kramer

General Research Corp.
ATTN: Dr. R. D. Hill

Georgia Tech.
ORA
ATTN: H. Denny

Grumman Aerospace Corp.
ATTN: J. Rogers, Dept. 533, PT 35

GTE Sylvania
Elec. Sys. Grp.
ATTN: C. Thornhill, Library

GTE Sylvania
ATTN: D. P. Flood

Harris Semicon.
ATTN: T. L. Clark, M.S. 4040

Hazeltine Corp.
ATTN: J. B. Colombo

Hercules, Inc.
ATTN: W. R. Woodruff, 100K-26

Honeywell, Inc.
Government & Aeronautical Products Division
ATTN: R. R. Johnson, A-1391

Honeywell, Inc.
Aerospace Division
ATTN: S. H. Graff, M.S. 725-5

DEPARTMENT OF DEFENSE CONTRACTORS (Continued)

Hughes Aircraft Co.
Space Systems Division
ATTN: E. C. Smith, Bldg. 366, M.S. C-E110

Hughes Aircraft Co.
Ground-Systems Group
ATTN: Library, Bldg. 600, M.S. C-222

Hughes Aircraft Co.
ATTN: B. W. Campbell, M.S. 6-E110

ITRI
ATTN: J. E. Bridges

ITRI
Elec. Comp. Anal. Ctr.
ATTN: ACOAT

Intelcom Rad Tech
ATTN: L. D. Cotler
ATTN: R. Stahl

IBM
ATTN: F. Frankovsky

IT&T
ATTN: F. Johnson, Def.-Sp. Grp., SMTS

Ion Phys. Corp.
ATTN: Dr. H. Milde

Johns Hopkins Univ.
Appl. Phys. Lab.
ATTN: P. E. Partridge

Kaman Sci. Corp.
ATTN: Dr. W. Ware
ATTN: O. Lopez

Litton Sys. Inc.
Data Sys. Div.
ATTN: S. Sternbach

Lockheed Missiles & Space Co.
ATTN: M-365, Dept. 81-23, Bldg. 154

LTV Aerospace Corp.
ATTN: TDC

LTV Aerospace Corp.
ATTN: T. M. Rozelle

MIT Lincoln Lab.
ATTN: L. Loughlin, Library

Martin Marietta Aerospace
ATTN: End. Lib., M. C. Griffith, MP-30

Martin Marietta Corp.
ATTN: D. M. Newell, MS-S0454

Maxwell Lab.
ATTN: Dr. V. Fargo

McDonnell Douglas Corp.
ATTN: C. G. Polak, E-411-107-1-D2

McDonnell Douglas Corp.
ATTN: R. J. DeBattista

DEPARTMENT OF DEFENSE CONTRACTORS (Continued)

McDonnell Douglas Corp.
ATTN: Library

McDonnell Douglas Corp.
ATTN: T. J. Lundregan

Mission Research Corp.
ATTN: D. E. Merewether

Mission Research Corp.
ATTN: Dr. C. L. Longmire

Mitre Corp.
ATTN: Library

Mitre Corp.
ATTN: L. D. Bickmoke

Motorola, Inc.
ATTN: TIC, A. J. Kordalewski

Northrop Corp.
ATTN: J. M. Reynolds

Northrop R&T Center
ATTN: Library

Northrop Corp.
ATTN: B. T. Ahlport

Pac-Sierra Research Corp.
ATTN: Sec. Ofc.

Perkin-Elmer Corp.
ATTN: T. D. Jones

Philco-Ford
WDL D
ATTN: Library

Philco-Ford A&C Ops.
ATTN: Dr. L. H. Linder

Phys. Internat.
ATTN: Dr. F. Ford

Pulsar Assoc.
ATTN: C. Jones

R & D Assoc.
ATTN: Dr. W. J. Karzas
ATTN: R. R. Schaefer

Rand Corp.
ATTN: Dr. C. Crain

Raytheon Co.
ATTN: G. Joshi, Rad. Sys. Lab.

Raytheon Co.
ATTN: J. R. Weckback

RCA Corp.
ATTN: E. Van Keuren, 13-5-2

RCA Corp.
ATTN: E. Daly

RCA Corp.
ATTN: Dr. G. Brucker

DEPARTMENT OF DEFENSE CONTRACTORS (Continued)

Rockwell Int. Corp.
ATTN: TIC, BA08

Rockwell Int. Corp.
ATTN: J. F. Sexton, CA31

Sanders Assoc.
ATTN: R. G. Despathy, Sr., PE, 1-6270

Science Applications, Inc.
ATTN: Dr. F. Tesche

Science Applications, Inc.
ATTN: N. R. Byrn

Science Applications, Inc.
ATTN: Dr. R. Beyster
ATTN: Dr. G. Stuart

Science Applications, Inc.
ATTN: Dr. B. Goplen

Simulation Physics, Inc.
ATTN: R. G. Little
ATTN: W. A. Seidler

Simulation Physics, Inc.
ATTN: A. J. Armini

The Singer Co.
ATTN: Dr. A. A. Wittels, M.S. 12-5820

Sperry Rand Corp.
UNIVAC Div.
ATTN: J. A. Inda, M.S. 5451

Sperry Rand Corp.
ATTN: C. Craig, EV

Stanford Research Institute
ATTN: Dr. R. A. Armistead

DEPARTMENT OF DEFENSE CONTRACTORS (Continued)

Stanford Research Institute
ATTN: H. Carey

Sundstrand Corp.
ATTN: C. White, Dept. 763SW

Systems, Science & Software
ATTN: A. F. Klein

Systron-Donner Corp.
ATTN: H. D. Morris

Texas Instruments, Inc.
ATTN: Dr. D. J. Manus, M.S. 72

TRW Systems Group
ATTN: J. E. Dahnke

TRW Systems Group
ATTN: W. H. Robinette
ATTN: TIC, S-1930

UAC
Norden Div.
ATTN: C. Corda

University of Denver
Colorado Seminary
ATTN: R. W. Buchanan

University of Arizona
Engineering Research Laboratories
5 cy ATTN: Dr. Robert Carlile

Varian Assoc.
ATTN: Dr. H. R. Jory, A-109

Westinghouse Electric Corp.
ATTN: H. P. Kalapaca, M.S. 3525